CHALCOGENIDE BASED ($CuInS_2$/ZnS, $CuInSe_2$/ZnSe) CORE/SHELL QUANTUM DOTS FOR PHOTODYNAMIC THERAPY

By

Armando Manuel Peña Duarte

A thesis submitted in partial fulfillment of the requirements for the degree of

MASTER OF SCIENCE
in
PHYSICS

UNIVERSITY OF PUERTO RICO
MAYAGÜEZ CAMPUS

2015

Approved by:

Maharaj Tomar, Ph.D President, Graduate Committee	Date
Dorial Castellanos-Rodríguez, Ph.D Member, Graduate Committee	Date
Sergiy Lysenko, Ph.D Member, Graduate Committee	Date
Omar Colón, Ph.D Representative of Graduate Studies Office	Date
Rafael Ramos, Ph.D Chairperson of the Department	Date

Abstract

Strong luminescent $CuInX_2/ZnX$ (X=S,Se) core/shell quantum dots were synthesized by a novel nontoxic and inexpensive organometallic method in two simple steps of $CuInS_2$ and $CuInSe_2$ core formation and ZnS and ZnSe shell over coating at 240° C, respectively. X-ray diffraction pattern confirms the $CuInX_2$ core and $CuInX_2/ZnX$ core/shell (X=S,Se). HR-TEM images revealed that the particle sizes is homogeneous and the $CuInS_2/ZnS$ and $CuInSe_2/ZnSe$ core/shell nanoparticles are pyramidal in shape by $CuInS_2$ and $CuInSe_2$ tetragonal phase with average diameters of approximately 4 nm to core and 6 nm to core shell structure. $CuInS_2/ZnS$ and $CuInSe_2/ZnSe$ core/shell quantum dots shown excellent photoluminescence properties with high fluorescence emission from 750 nm to 850 nm. Quantum confinement effects were observed for red and Near-IR emission and quantum yield increasing form 11% to 62% after ZnSe overcoating for ternary chalcopyrites of $CuInSe_2$. The $CuInSe_2/ZnSe$ core/shell quantum dots synthetized were used as photosensitizers in the production of ROS such as $^1O_2$, since selenium has long been viewed as having anticancer effects based on early numerous experiments from animal models. The kinetic study of the singlet oxygen quenching reaction with 1,3-diphenylbenzofuran, was conducted by the photoluminescence emission intensity decrease. Here we report $CuInSe_2/ZnSe$ core/shell quantum dots revealed characteristics of a sensitizer nanoparticle produce reactive oxygen species such as singlet oxygen ($^1O_2$), it shown for a promising application in the photodynamic therapy and optical device application as photosensitizer in ROS production, as well as biosensors.

Keywords. $CuInS_2/ZnSe$, $CuInSe_2/ZnSe$, Core/Shell, Quantum Dots, Photoluminescence**,** Single Oxygen, Photodynamic therapy

Resumen

$CuInX_2/ZnX$ (X=S,Se) core/shell quantum dots (QDs) con alta luminiscencia fueron sintetizados mediante un nuevo método no tóxico y eficiente, el cual se basa en dos pasos de reacción: uno para estructuras del núcleo o "core"de $CuInS_2$ y $CuInSe_2$ y, el otro, para el cascarón o "shell" de ZnS y ZnSe a 240°C. Se evidenció mediante XRD la formación de las estructuras $CuInX_2$ core y $CuInX_2/ZnX$ core/shell (X=S,Se). Imágenes de HR-TEM muestran homogeneidad en el tamaño de partícula de ambos sistemas y evidencian la estructura piramidal de las calcopiritas que conforman el núcleo $CuInS_2$ y $CuInSe_2$ de los sistemas respectivos. Ambos sistemas muestran excelentes propiedades de emisión de fotoluminiscencia entre los 750 nm y los 850 nm. Los efectos de confinamiento cuánticos fueron observados en las regiones de emisión en el rojo y el IR cercano. El rendimiento cuántico se incrementó del 11% al 62% después de realizar el recubrimiento con ZnSe. Los QDs CuInSe2/ZnSe core/shell sintetizados fueron utilizados como foto-sensibilizadores en la producción de ROS tales como $^1O_2$. El estudio cinético de la reacción de bloqueo del oxígeno singlete con 1,3-diphenylbenzofuran, se comprobó por la disminución de la intensidad de emisión de fotoluminiscencia del DPBF. Los estudios cinéticos con CuInSe2/ZnSe core/shell QDs revelaron características de sensibilizador para producir especies reactivas del oxígeno tales como el oxígeno singlete ($^1O_2$). Estos resultados permiten plantear la aplicación de CuInSe2/ZnSe core/shell QDs en la terapia fotodinámica, como fotosensibilizador en la producción de ROS, en el desarrollo de dispositivos ópticos y biosensores.

Palabras clave: $CuInS_2/ZnSe$, $CuInSe_2/ZnSe$, Core/Shell, Quantum Dots, fotoluminiscencia, oxígeno singlete, terapia fotodinámica

A Lorinda, Julia, Aranza, Andreína, Aníbal, Fátima...

Acknowledgments

To "God" for "my sense-eight..."

To the University of Puerto Rico at Mayagüez, specially to Department of Physics, for giving me the opportunity to develop as a student and researcher.

To the IRG2 project: Engineered Non-Toxic Quantum Dots Systems for Cancer Therapy Applications" NSF-CREST-UPRM. National Science Foundation (NSF), Center for Research Excellence in Science and Technology (CREST) at the University of Puerto Rico at Mayagüez (UPRM); for funding support.

To my advisor, Dr. Maharaj S. Tomar, for his support, guidance, motivation, scientific discussions, and the opportunity to work in his laboratory.

To Dr. Luis Rivera, for their support in the measurements and scientific discussions at Department of Chemistry at UPRM.

To Dr. Oscar Perales, for their support in the measurements and scientific discussions at The NANO materials Processing Laboratory at UPRM

To Dr. Arun Kumar, for his support and scientific discussions.

To Sr. Oscar Resto UPR-RP, for the TEM images at the IFN Nanospectroscopy Laboratory UPR-RP.

To my f***amily***.

To Gina Montes, I love you… Namaste!

To people or energies who made it possible.

Thank you!

TABLE OF CONTENTS

TABLE OF FIGURES

1. INTRODUCTION

A quantum dot (QD), likewise named colloidal semiconductor nanocrystal, is a semiconductor material nanostructured with a discrete quantized energy spectrum. QDs semiconductor nanoparticles bidding scientific attention due to their size and shape reliant on properties.[1-5] QDs has been synthetized of an photoluminescent inorganic core like CdS, CdSe, CdTe,[5,6] composed of a few hundred atoms, surrounded by an organic external layer of surfactant ligands. Photoluminescent QDs semiconductor nanostructures are considered as photosensitizer in photodynamic therapy, fluorescence marker for biomolecules[3-5] and absorber material for solar cells[6, 9] or light emitting diode[10], due to their tunable absorption and emission in the visible and infrared range of the solar spectrum. Nevertheless, the best considered materials until now, like cadmium and lead chalcogenides, have a disadvantage of containing highly toxic constituents that limits their potential applications.[11, 12]

Potential alternatives less toxic materials that have been used, and having a tunable absorption in the visible range, are copper indium chalcogenides. These chalcogenides in the bulk material have a direct band gap semiconductor approximately 1.5eV, a high radiation, an exciton radius of 4 nm,[13] and an extinction coefficient of 105 cm^{-1} around of 500 nm.[14] Consequently, cupper indium chalcogenides are at present broadly used in thin film solar cells conventionally prepared by sputtering or evaporation techniques.[15] In contrast, there are a small number of studies about organometallic synthesis of colloidal cupper indium chalcogenides nanoparticles with a close size distribution and efficient size or shape control.

QDs confines excitons (bound pairs of conduction band electrons and valence band holes) in all three spatial dimensions. As a consequence of this confinement, QDs involved abundant attention for their novel characteristics like properties such as lower band gap than bulk semiconductor. One way of producing confinement is to build an interface between different semiconductor materials by creating a core/shell QDs system. Association of semiconductors with other materials such as metals, oxides, sulfides, *etc*., in the same heterostructure, constitutes a quantum well system, which allows for the design of core/shell QDs, combining different physical properties such as fluorescence, magnetism, and different decay lifetimes.

Since last decades, there has been applied the effective mass approximation to calculate the electronic structure of quantum-dot and quantum wells semiconductors (QDQWS) generated by difference between electrostatic potentials in interface of core and shell heterostructure. Electronic structure of QDQWS was assessed for evaluation of the electron and hole waves functions, the 1*s* transition energy, and the overlap of wave functions.[16,17]

1.1.Background

In earlier works has been synthetized cadmium and sulfide based CdS/ZnS[6] and chalcogenides $CuInS_2$[13,14] core and $CuInS_2$/ZnS[15], core/shell quantum dots with high photoluminescent properties, but these materials can be degrade slowly inside of organism generating high toxic cadmium ions and sulfide ions and consequently hydrogen sulfide, which one are high toxic in cell environment. This problem can be resolve with change of sulfide ion by selenide ion in the core/shell nanoparticles to form $CuInSe_2$/ZnSe. Selenium has long been viewed as having anticancer effects based on numerous experiments from

animal models, human chemopreventive efficacy using Se supplement in human, and anticancer activity of selenoproteins systems evaluation.[18]

ZnSe could be a very good candidate as a shell material due to its wider band gap (E_g =2.69 eV) than that of $CuInSe_2$ (1.04 eV) and the band orientation is of type I, *i.e.*, both electrons and holes are confined in $CuInSe_2$.[19] Previous works in which ZnSe was used as shell in nanostructures of core/shell type, exhibited quantum yields (QYs) ranging from 60 to 85% and narrow emission line widths.[20, 23] Hence, different compositions of core/shell structures have been used.[15,16,24]

Novel functional heterostructures of $CuInSe_2$/ZnSe core/shell QDs can be generated for applications in several fields such as, optoelectronics devices, solar cells, aerospace engineering and healthcare. In most of these areas, the $CuInSe_2$/ZnSe core/shell QDs are used as a stage for additional surface functionalization, boosting their solubility in different media, increasing the ability to adjust their assembly properties on particular substrates or induce their binding to other molecules or macromolecules.[6, 25, 26]

1.2.Motivation

All these modifications opened up new areas with major interest of application of core/shell QDs such as photodynamic therapy (PDT).[27, 28] PDT is a relatively new method for cancer treatment, where tumor cells are exterminated by light-induced confined production of a reactive oxygen species (ROS), such as singlet oxygen ($^1O_2$) and other radical species such as superoxide anion radical ($O_2^{\circ-}$).[29] In general, core/shell QDs or others nanometric semiconductors could be used in PDT as photosensitizers, carriers of

photosensitizing molecules, magnetic nanoparticles, up- and down- converters for photosensitizing molecules, molecular targeting nanostructures, *etc*.[30-34]

In this context, we a novel approach the synthesis and characterization of copper indium chalcogenides core/shell quantum dots ($CuInS_2$/ZnS and $CuInSe_2$/ZnSe) by a novel and sustainable two-steps reaction of copper, indium salts, selenium powder sources and zinc salts with very low toxicity. The $CuInSe_2$/ZnSe core/shell quantum dots synthetized were used as photosensitizers in the production of ROS such as $^1O_2$.[32, 34] The singlet oxygen generated *in situ* from the CuInSe2/ZnSe core/shell quantum dots was determined by an indirect chemical quenching using 1,3-diphenylbenzofuran (DPBF). The kinetic study was performed by following the decrease of the DPBF photoluminescence (PL) emission with time.[35-39] $CuInSe_2$/ZnSe synthesis was based on previous studies to obtain sulfur chalcogenides. [6, 40, 41]

1.3.Objectives

1.3.1. Main Objective

The main objective of this work is to synthesize and to study the optoelectronic performance of chalcogenide based ($CuInS_2$, $CuInSe_2$, $CuInS_2$/ZnS, $CuInSe_2$/ZnSe) core/shell quantum dots for phodynamic therapy.

1.3.2. Specific Objectives

1.3.2.1. Synthesize indium chalcogenides core/shell quantum dots ($CuInS_2$, $CuInSe_2$, $CuInS_2$/ZnS, $CuInSe_2$/ZnSe) by a novel and sustainable two-steps reaction of copper, indium salts, and sulfur or selenium sources and zinc salts with very low toxicity.

1.3.2.2. Characterize structural properties of the nanoparticles ($CuInS_2$, $CuInSe_2$, $CuInS_2/ZnS$, $CuInSe_2/ZnSe$) through X-ray diffraction, transmission electron microscopy, and high resolution transmission electron microscopy.

1.3.2.3. Characterize optical properties of QDs ($CuInS_2$, $CuInSe_2$, $CuInS_2/ZnS$, $CuInSe_2/ZnSe$) by photoluminescence measurements.

1.3.2.4. Determine $CuInSe_2/ZnSe$ Photosensitizing Properties and singlet oxygen generation *in situ* from by an indirect chemical quenching using 1,3-diphenylbenzofuran (DPBF).

2. MATERIALS AND METHODS

2.1.Materials

Copper(I) acetate (CuOAc, 97%, Sigma-Aldrich), indium(III) acetate ($In(OAC)_3$, 99%, Alfa Aesar), 1-dodecanethiol (DDT 98%, Acros Organics), selenium powder (99.99%, Sigma-Aldrich), zinc acetate dihydrate (98%, Acros Organics), tri-n-octylphosphine (TOP, 97%, Sigma-Aldrich), trioctylphosphine oxide (TOPO, 99%, Sigma-Aldrich), oleylamine (OA, 70%, Sigma-Aldrich), 1-octadecene (ODE, 90%, Acros Organics), and nitrogen (high purity, 99.98%) were used as precursor for synthesis $CuInS_2$/ZnS and $CuInSe_2$/ZnSe core/shell structures.

2.2.Core and Core/shell Synthesis

$CuInS_2$ and $CuInSe_2$ core were synthesized through the reaction of 0.2mmol of 1-dodecanthiol and selenium powder, respectively, with 0.1mmol of CuOAc, 0.1m mol of $In(OAc)_3$, 5mL of tri-n-octylphosphine, 0.5mmol of trioctylphosphine oxide, 5mL of oleylamine, and 10mL of octadecene, at 250°C, in nitrogen atmosphere. After core being 60 min in reaction temperature, it was cooled to room temperature and 20 ml of ZnS and ZnSe precursors were added by pressure-equalizing dropping funnel, to respective $CuInS_2$ or $CuInSe_2$ core structures. Then, temperature was increased to 240° C ZnS or ZnSe shell over coating and the reaction was continued for an additional 30 minutes and finally cooled to room temperature. For precipitating ethanol and acetone was added followed by centrifuging (8000 rpm). The QD structures were suspended in hexane and precipitated in a mixture ethanol: acetone 5:1, this process was repeated three times to remove unreacted materials. Finally, the precipitated product was suspended in hexane. ZnS precursor was prepared by mixing a solution of 2mmoles of thiourea powder in 10 mL of tri-n-

octylphosphine and a solution of 2mmoles of zinc acetate in 10mL oleylamine with vigorous stirring.[6, 40] ZnSe precursor was prepared by mixing a solution of 2mmoles of Se powder in 10 mL of tri-n-octylphosphine and a solution of 2mmoles of zinc acetate in 10mL oleylamine with vigorous stirring.[6, 40, 41]

2.3.Characterization

Structural characterization by means of powder X-ray diffraction was carried out on a Siemens D500 diffractometer using a high-power Cu-kα source operating at 50 kV and 35mA with a Kevex solid-state detector. Average crystallites sizes were calculated using the main diffraction peaks and according to Scherrer's equation.[42] To calculate the relative intensity the following equation was used:

$$RI = \frac{I_i}{I_{Max}} x100$$

The Bragg's Law was used to calculate the crystal diameter. The Bragg's Law is as follows:

$$d = \frac{n * \lambda}{2 * \sin(\theta)}$$

The crystal size was calculated by Scherrer's equation as follows:

$$Size = \frac{0.9 * \lambda}{FWHM * \cos(\theta)}$$

Where:

I_i: intensity of *i*-peak
I_{Max}: maximum intensity peak
n: 1, K_α
λ Cu_α: 1.541838 Å
FWHM: full width at half maximum calculate by PowderX®

The presence of adsorbed surface species was determined using Fourier Transform Infrared technique, using a Shimadzu IR-Afinity spectrometer. The materials were

examined using a on a JEOL-2011 and a JEM-ARM200F high resolution transmission electron microscope, also equipped with an x-ray energy dispersive spectrometer. The optical properties were measured using a Fluoromax2 Photo-spectrometerspectrophotometer for photoluminescence measurements. The excitation wavelength for photoluminescence measurements was set at 400nm. PL Quantum Yield (QY) of QDs was calculated by comparing their integrated emission to that of rhodamine B, QY = 90% in absolute ethanol with λ_{ex} = 515 nm at 10 °C. All optical measurements were performed at room temperature. High Resolution Transmission Electronic Microscope (HRTEM) (JEOL transmission microscopy, model JEM-2100, 200KV) was employed to characterized morphology and structure of core/shell structures. Elemental compositions of QDs were determined by energy-dispersive spectroscopy (EDS). Films of samples were studied in Shimadzu FTIR-8400: Fourier Transform Infrared Spectrophotometer Shimadzu FTIR-8400.

2.4.Singlet Oxygen Characterization

A suspension of 1.0 mL of DPBF 1.02×10^{-6} mol/L and 0.1 mL of QDs $1.\times10^{-6}$ mol/L were mixed and diluted to 10mL in hexane. The mixture was continuously irradiated by a fluorimeter´s lamp during all analysis. After the irradiation, the solution was tested in the same instrument and PL measurements were taken each 30 seconds at room temperature. The relative fluorescence intensity of the solution was measured at 447 nm with excitation at 403 nm. DPBF is highly sensitive to the presence of reactive oxygen species such as singlet oxygen. PL intensity was measured 9 times by sample, generating a standard deviation of 2.2% .[32-39]

3. RESULTS AND DISCUSSION

3.1. $CuInS_2$/ZnS core/shell QDs system

3.1.1. Structural Characterization

The structural phases of $CuInS_2$ core and $CuInS_2$/ZnS core/shell structure were acquired by means of X-ray diffraction (XRD) characterizations. Figure 1 shows the XRD patterns of the $CuInS_2$ core and $CuInS_2$/ZnS core/shell nanoparticles synthesized. The diffraction peaks can be indexed to the (112), (204)/(220), and (116)/(312) reflections of the tetragonal crystal structure of $CuInS_2$ chalcopyrite phase.

The formation of the $CuInS_2$ zincblende phase can be reason of absent of diffraction peak of (200) characteristics of zincblende phases. With $CuInS_2$ coated with the ZnS shell, peaks exhibited a shift to greater angles, closer to the characteristic peak location of bulk cubic ZnS. $CuInS_2$/ZnS core/shell peaks are less wide and are more defined than peaks of $CuInS_2$ core doubt to a possible increased particle size.

The Scherrer equation was used to determine the size of $CuInS_2$ core and $CuInS_2$/ZnS core/shell QDs, the average diameters calculated were 5.0nm and 6.5nm, respectively, with ±0.5nm of error. We used the Scherrer constant of 0.89 for tetrahedral structures perpendicular to the plane (111) in cubic phase, due this equals to (112) plane of tetragonal phase.[22, 42, 43]

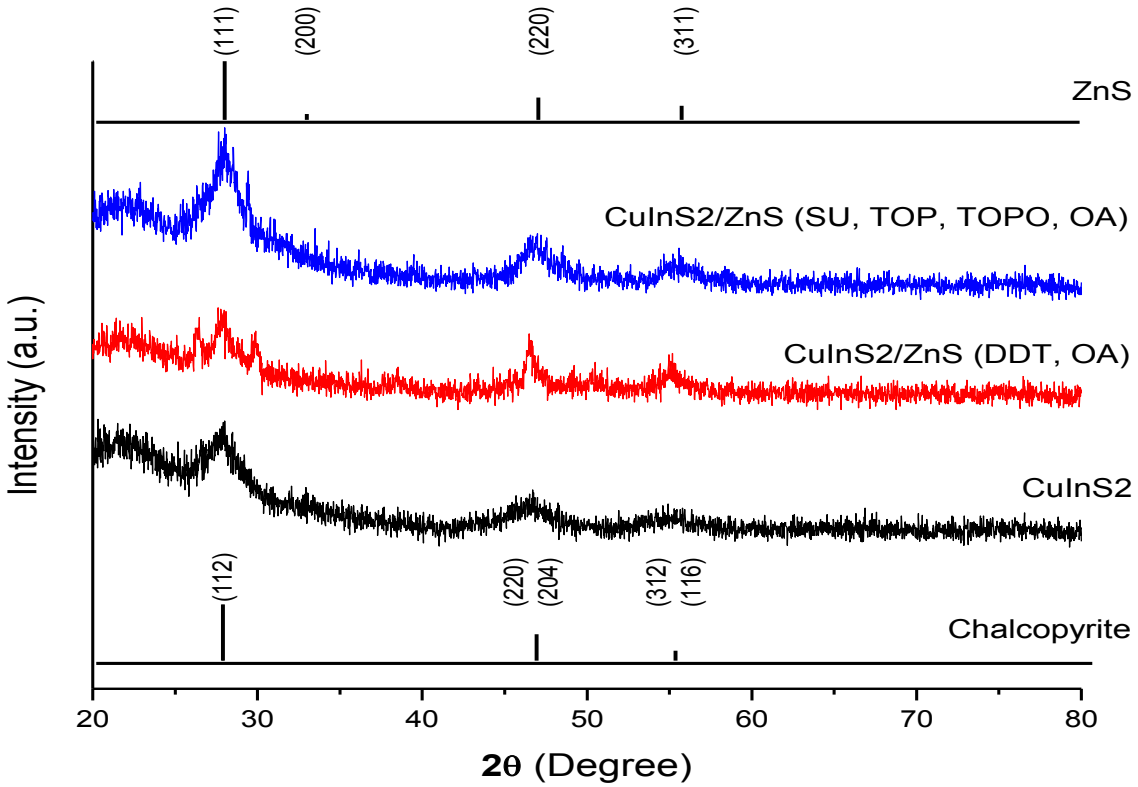

Figure 1. XRD patterns of JCPDS chalcopyrite, ZnS, $CuInS_2$ core and $CuInS_2$/ZnS core/shell quantum dots synthesized by two methods different: DDT and OA

HR-TEM images, figure 2, reveal that the particle sizes of the $CuInS_2$/ZnS core/shell nanoparticles are significantly pyramidal in shape by $CuInS_2$ tetragonal phase, with diameters of approximately 5nm, and have homogeneous particle size distribution. HR-TEM images reveal that the particle sizes of the $CuInS_2$/ZnS core/shell nanoparticles are significantly pyramidal in shape by $CuInS_2$ tetragonal phase, with diameters of approximately 5nm, and have homogeneous particle size distribution.

The figure 2f show the organization of chalcogenide clusters with ligands propose by Zhong *et al.*[13] The average diameter of $CuInS_2$ core and $CuInS_2$/ZnS core/shell QDs, obtained by HRTEM, were 5nm and 6nm, respectively, with ±1nm of error.

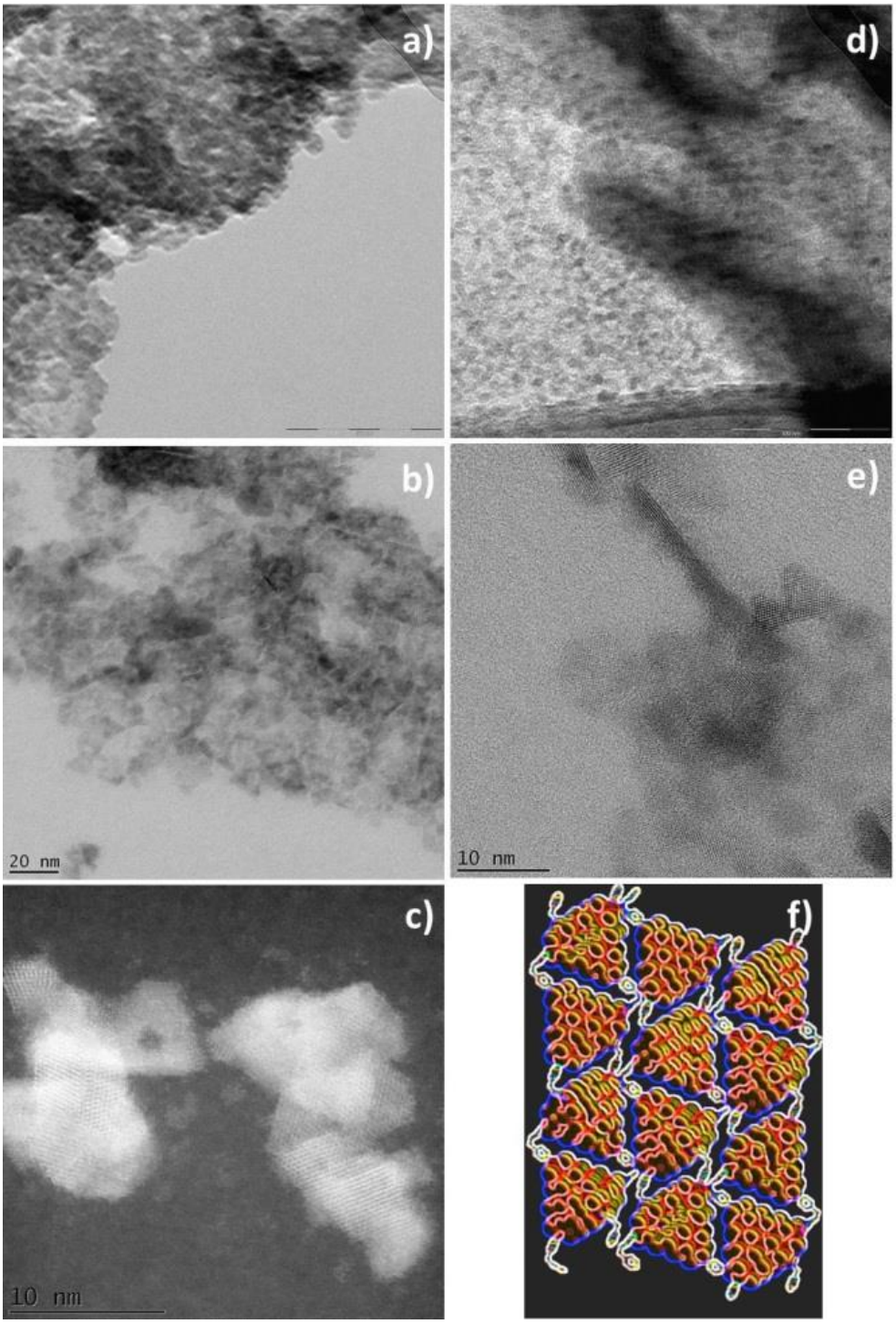

Figure 2. TEM and HRTEM micrographs of $CuInS_2$/ZnS core/shell quantum dots synthesized by SU-TOP-TOPO-OA method (a, b, c), DDT-OA method (d, e), and schematic model (f) of NP aggregation[13]

3.1.2. Optical Properties

PL spectra of $CuInS_2$ core and $CuInS_2$/ZnS core/shell quantum dots synthesized by two methods different are showed in Figure 3. The study of photoluminescence core/shell nanoparticles reveal excellent photoluminescent (PL) properties with emission observed for red and Near-IR regions, approximately 725nm and 735nm for DDT and OA methods, respectively. The small PL spectra width could indicate a homogeneous size distribution for $CuInS_2$ and $CuInS_2$/ZnS QDs, supporting the results of HR-TEM method. Nevertheless, previous works in chalcogenides synthesis had reported broadening of photoluminescence spectra peaks. In the literature, there are not reported peak width smaller 60 nm for $CuInS_2$. Synthesis methods of CuSe and monodispersed colloidal spheres for uniform Y_2O_3:Eu^{3+} have reported PL spectra peak width shrink until 40nm and 10nm, respectively. Moreover, calibration of the instrument used in determining PL measures could directly influence the width of any spectrum peak photoluminescence.

Relating both methods we observe a difference in the luminescence emission intensity[17,20-23, 40]. PL intensity decreases when we use SU-TOP-TOPO-OA instead of DDT-TOP-TOPO -OA. In the spectrum it can also be observed a slight shift toward a longer wavelength, when the synthesis is performed without DDT.

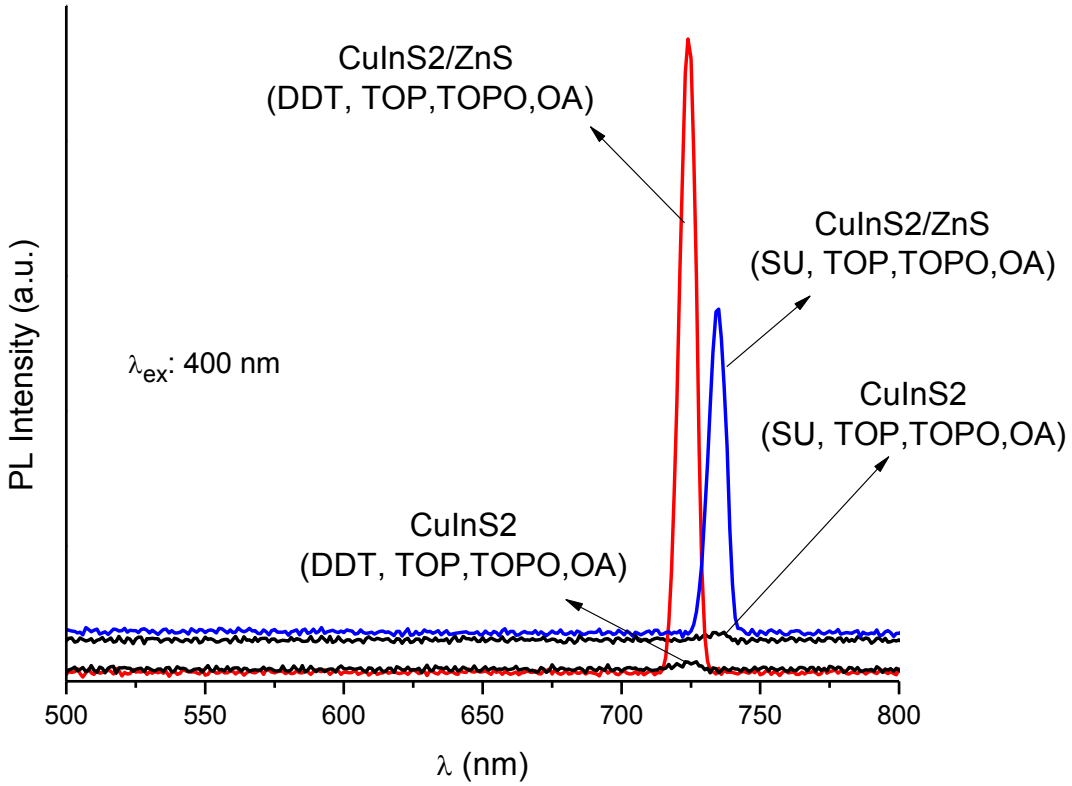

Figure 3. PL spectra of $CuInS_2$ core quantum dots and $CuInS_2$/ZnS core/shell quantum dots synthesized at 250°C, with excitation at 400nm. PL intensity were much higher than that for $CuInS_2$ due to the fact that the ZnS shell growth diminishes the number of surface interactions or bounds, which can develop as trap states for charge carriers and thus reduces the optical properties[4]

Original ligand molecules on the $CuInS_2$/ZnS core/shell QDs surface can be exchanged by others, which can produce diverse properties to the nanoparticles, such as luminescence diminishes and optical changes. Primary quantities of OA have been exchanged with thiols containing different functional groups, which can interact with $CuInS_2$/ZnS nanoparticle surface. A quenching effect generated by pi-bonding in the structure of OA, it could be cause of luminescence diminishes in $CuInS_2$/ZnS core/shell QDs synthetized by DDT route.

Quantum confinement effects were observed for red and Near-IR emission and quantum yield increasing form 9% to 47% after ZnS overcoating for ternary chalcopyrites.

$CuInS_2$/ZnS core/shell nanoparticles synthetized have attracted great attention for their exceptional PL properties which is promising in applications as photodynamic therapy[16-23, 40].

3.1.3. Partial conclusions for $CuInS_2$/ZnS core/shell QDs system

1. $CuInS_2$ core and $CuInS_2$/ZnS core/shell QDs were synthesized using DDT and SU with excellent PL properties.
2. Capping exchange with thiol molecules results in an increased luminescence efficiency for $CuInS_2$/ZnS QDs.
3. Quantum confinement effects were observed for red and Near-IR emission, as predicted by their small diameter (~5 nm) compared to the bulk Bohr radius.
4. QDs synthetized have attracted great attention for their optical properties which is promising in applications as photodynamic therapy and solar cells.

3.2.$CuInSe_2$/ZnSe core/shell QDs system

3.2.1. Structural Characterization

A new, simple and sustainable method of synthesis of $CuInSe_2$/ZnSe core/shell QDs, the $CuInSe_2$ core quantum dots was developed matrix synthesis cooled and added slowly with constant stirring in inert atmosphere, the precursors ZnSe were added by pressure-equalizing dropping funnel with the temperature was slowly increased to 240°C. This method of synthesis could prevent the formation of agglomerates and facilitate the formation of shells with better size distribution, due to the previous surrounding and probable solvation of the $CuInSe_2$ core by the precursor molecules of ZnSe. Some author proposed the $CuInSe_2$ nanoparticles, can serve as catalyzer and nucleation center.[12, 20, 21]

The structural phases of $CuInSe_2$ core and $CuInSe_2$/ZnSe core/shell structure were acquired by means of X-ray diffraction (XRD) characterizations. (Figure 4) shows the XRD patterns of the $CuInSe_2$ core and $CuInSe_2$/ZnSe core/shell nanoparticles synthesized. The diffraction peaks can be indexed to the (112), (204)/(220), and (116)/(312) reflections of the tetragonal crystal structure of $CuInSe_2$ chalcopyrite phase. The development of the $CuInSe_2$ zincblende phase can be excluded doubt the absence of diffraction peak of (200), distinguishing peak of zincblende phases. After the sample was coated with the ZnSe shell, all peaks exhibited a mild shift to larger angles, closer to the characteristic peak setting of bulk cubic ZnSe. The $CuInSe_2$/ZnSe core/shell QDs peaks are less wide and are more defined than peaks of $CuInSe_2$ core, its indicating increased particle size.

The Scherrer equation was used to determine the size of $CuInSe_2$ core and $CuInSe_2$/ZnSe core/shell QDs, the average diameters calculated were 3.6nm and 5.5nm,

respectively, with ±0.5nm of error. We used the Scherrer constant of 0.89 for tetrahedral structures perpendicular to the plane (111) in cubic phase, due this equals to (112) plane of tetragonal phase.[22, 42, 43]

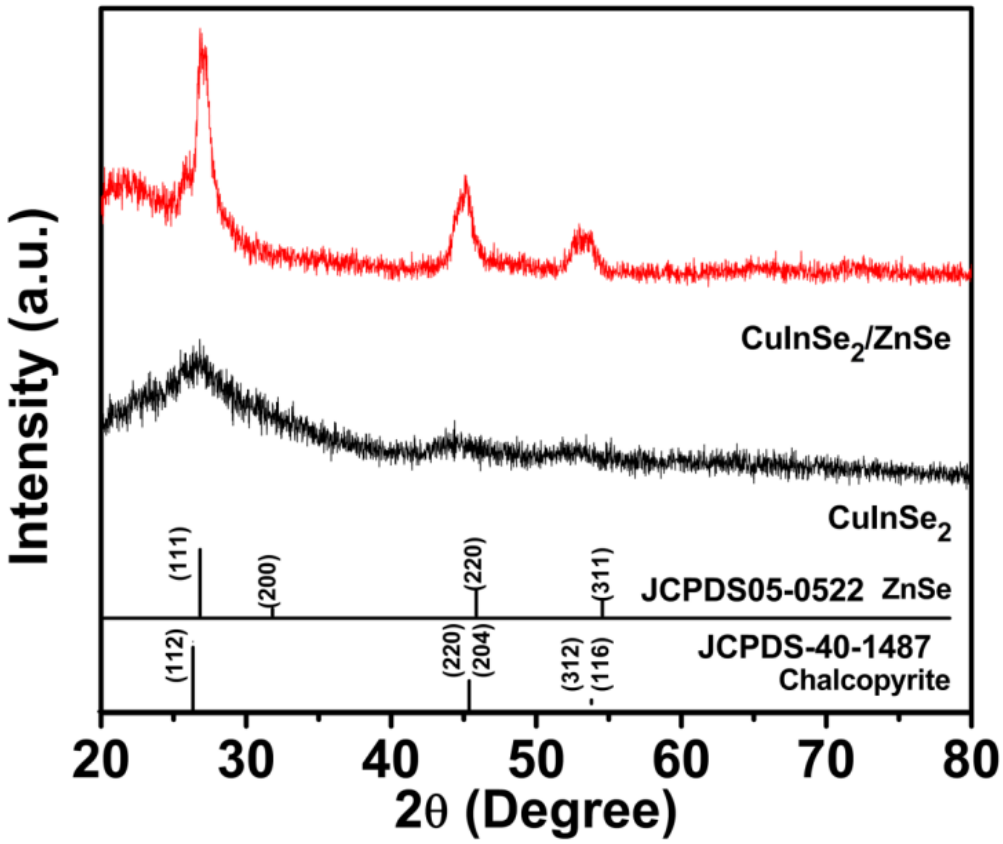

Figure 4. XRD patterns of $CuInSe_2$ core and $CuInSe_2$/ZnSe core/shell quantum dots synthesized. The XRD patterns for bulk $CuInSe_2$ (JCPDS 40-1487) and ZnSe (JCPDS 05-0522) are shown as reference. Synthesized $CuInSe_2$/ZnSe core/shell QDs peaks are less wide and are more defined than peaks of $CuInSe_2$ core, indicating increased particle size: the Scherrer average diameters calculated were 3.6nm and 5.5nm, to $CuInSe_2$ core and $CuInSe_2$/ZnSe core/shell QDs, respectively, with ±0.5nm of error.

The crystalline structure of the $CuInS_2$/ZnS core/shell quantum dots was revealed by using high-resolution transmission electron microscopy (HRTEM) shown in (Figure 5). Based on the evidence found with the HRTEM analysis, the observed lattice fringes with a distance of 0.334 nm can be associated to the (112) plane of the chalcopyrite phase. All $CuInSe_2$ pyramids sides should be (111) surface, supposing the $CuInSe_2$ pyramids are of

zincblende phase with distance lattice spacing of 0.334 nm, which indicates the chalcopyrite phase of $CuInSe_2$ pyramids. Lattice parameters of 0.334 nm and 0.206 nm matches (112) and (220) planes of the $CuInSe_2$ chalcopyrite phase. $CuInSe_2$ core QDs show trigonal pyramidal shape related to the polarity and stability of chalcopyrite surface sides. The (112) plane of the $CuInSe_2$ tetragonal phase is a polar surface, which have positive or negative terminated surface. These polar sides have a higher surface energy and high reactivity. The fast growth along the [112] direction normally diminishes the (112) plane, leaving non-polar surfaces such as (114) planes. The constant lattice spacing and clear crystal planes evidence the crystal morphology of $CuInSe_2$ core $CuInSe_2$/ZnSe core/shell structures.[44,45] The average diameter of $CuInSe_2$ core and $CuInSe_2$/ZnSe core/shell QDs, obtained by HRTEM, were 4nm and 6nm, respectively, with ±1nm of error (see supporting information in Figure S1, S2 and S3).[46,47]

The Fourier-transform infrared (FT-IR) spectra of $CuInSe_2$/ZnSe core/shell QDs synthesized are shown in supporting information (see figure S4). It is shown that distinct absorption peaks are observed at (2858, 2954,3261, 3423)cm^{-1}, which corresponds to $CuInSe_2$, and (1380, 1614)cm^{-1} The FTIR spectra of $CuInSe_2$/ZnSe core/shell QDs show several peaks for typical organic compounds such as methyl, methylene, and methine groups (CH_3, CH_2, CH, respectively) and nitrogenous substances presents in ligands structures used. The broad and strong band near 3261 cm^{-1} and 3423 cm^{-1} represents asymmetric stretching of amine groups. The band near 2900 cm^{-1} characterizes —CH stretching mode of —CH_2 group. The bands near 1460 cm−1 and 1380 cm^{-1} are attributed to — CH_3 bending and —CH_3 shaking respectively. The band at 1000 cm^{-1} is attributed to —CH_3 rocking and —CH_2 shaking modes. The C–P stretching peaks of TOP appeared at

1170, 1076 and 1,032 cm^{-1}. The peak at 728 cm^{-1}related with (–CH2–)n ($n \geq 4$) stretching of TOP was also observed. From these data, it could be confirmed that the TOP was successfully capped on the $CuInSe_2$/ZnSe core/shell QDs surface.[48,49]

3.2.2. Optical Properties

Excellent photoluminescence (PL) properties with emission observed for red and Near-IR regions, approximately at 800 nm (Figure 6). PL intensity, photostability and photoluminescence QY of $CuInSe_2$ QDs were considerably enhanced by means of the growth of a shell of ZnSe of higher band gap value.[22, 23, 40]

The small PL spectra width could indicate a homogeneous size distribution for $CuInS_2$ and $CuInSe_2$/ZnSe QDs, supporting the results of HR-TEM method. Nevertheless, previous works in chalcogenides synthesis had reported broadening of photoluminescence spectra peaks. In the literature, there are not reported peak width smaller 60 nm for $CuInSe_2$. Synthesis methods of CuSe and monodispersed colloidal spheres for uniform Y_2O_3:Eu^{3+} have reported PL spectra peak width shrink until 40nm and 10nm, respectively. Moreover, calibration of the instrument used in determining PL measures could directly influence the width of any spectrum peak photoluminescence.

ZnSe has chemical stability and nontoxic large semiconductor band gap, exhibiting a type-I semiconductor. When it overcoats the $CuInSe_2$ core, the lattice mismatch between $CuInSe_2$ core and ZnSe shell is relatedly low as in the case of $CuInS_2$/ZnS systems (around 2%).[20-23, 40] A strong enhancement of the PL intensity in the emission peak of $CuInSe_2$ can be observed in (Figure 6), when it is coated with ZnSe shell. The QY of synthetized QDs

increased from 11% to 62% and is highest (to our knowledge) for ternary chalcopyrites.[6,15,20,25,40]

These PL properties suggest the possibility of using these structures in different areas such as light-emitting devices, solar cells, fluorescent biological labeling or, more specifically, a kind of photosensitizer nanoparticle in singlet oxygen generation exhibiting promising application in the PDT. The narrow peak width of the PL intensity in the (figure 6) infer on the homogeneous distribution and small particle size, supporting the results of XRD and HR-TEM methods. There is a shift of band gap energy where is the PL maxima intensity of $CuInSe_2$ bulk, from 1.07 eV to 1.55eV (1.55 eV or 800 nm). This shift is due to Bohr exciton radios.[16,17]

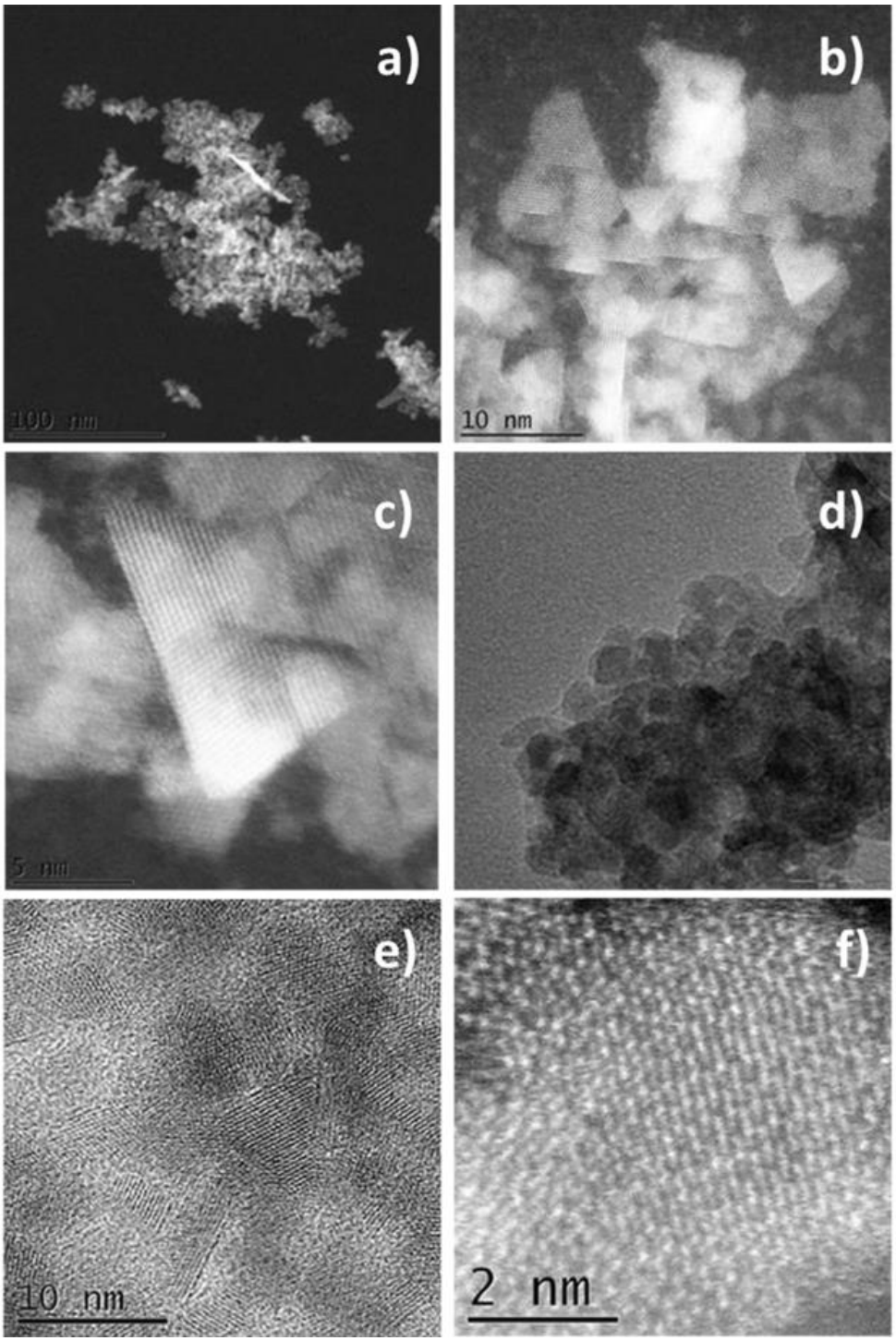

Figure 5. TEM and HRTEM $CuInSe_2$ core QDs and $CuInSe_2$/ZnSe core/shell QDs synthesized at 250°C, with average diameter, obtained by HRTEM, were 4nm and 6nm, respectively, with ±1nm of error: a, b) and c) HRTEM $CuInSe_2$ core QDs with three different magnifications, d) TEM of $CuInSe_2$/ZnSe core/shell QDs, e) and f) HRTEM of $CuInSe_2$/ZnSe core/shell QDs with tow different magnification show interphase between $CuInSe_2$ core and ZnSe shell. HRTEM analysis show $CuInSe_2$ core QDs show trigonal pyramidal shape related to the polarity and stability of chalcopyrite surface sides.

Theoretical and experimental studies have shown the nanoparticle size dependent optical band gap of the chalcopyrite-type ternary I-II-VI_2 semiconductor QDs. Based on the nanoparticle size dependent optical band gap reported for ternary chalcopyrite, it was shown that the optical band gap of QDs covers wide wavelength range from near-infrared to ultraviolet.[16-21]

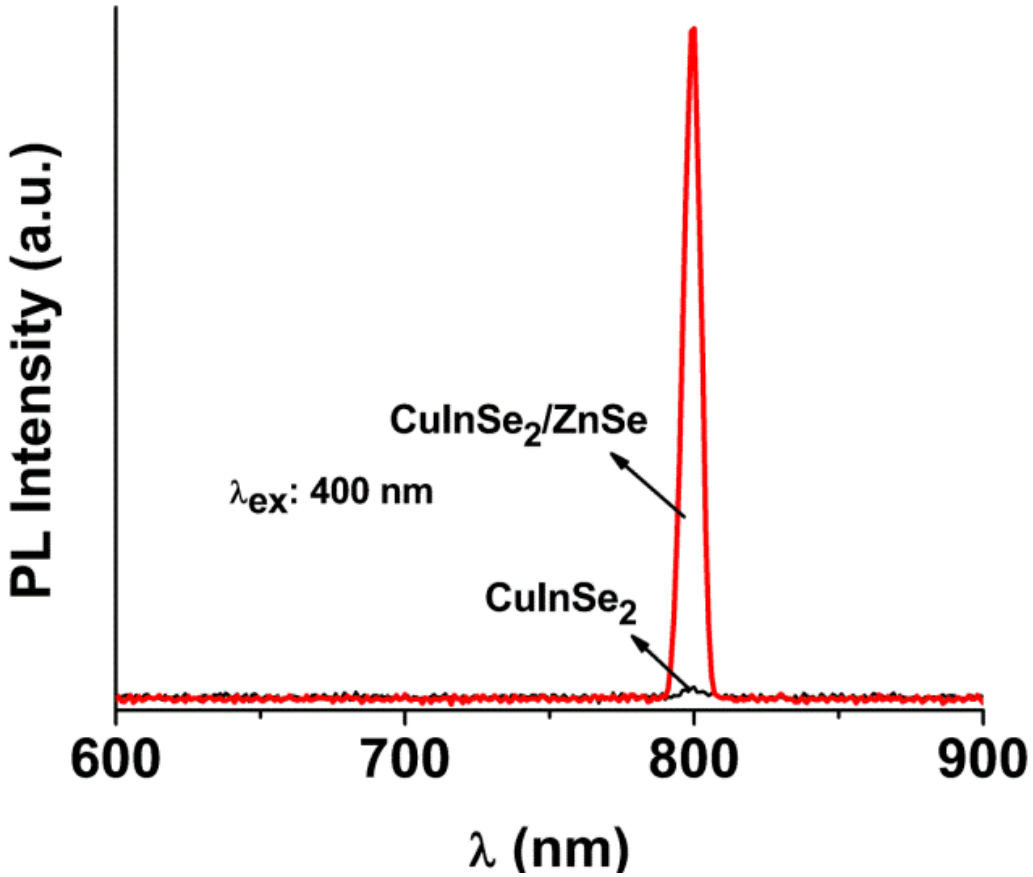

Figure 6. PL spectra of $CuInSe_2$ core quantum dots and $CuInSe_2$/ZnSe core/shell quantum dots synthesized at 250°C, with excitation at 400nm. PL intensity and QY of $CuInSe_2$/ZnSe (62%) were much higher than that for $CuInSe_2$ core (11%),due to the fact that the ZnSe shell growth diminishes the number of surface interactions or bounds, which can develop as trap states for charge carriers and thus reduces the optical properties.

3.2.3. $CuInSe_2$/ZnSe Core/Shell Quantum Dots As Semiconductor Type-I.

Band gaps, effective masses, composition and relative electronic energy levels difference between the core and the shell, the core diameter and the shell thickness, materials bring about either type I or type II semiconductor structures. Type I assembly corresponds to the condition in which both a hole and an electron are located in the same section of the heterostructure, the core or the shell side. In the type II arrangement holes and electrons are physically separated and reside in different regions in the core/shell structure. Preliminary studies have focused on type I core/shell QDs, in which the shell is used to passivate the surface of the core with the goal to improve photoluminescence quantum efficiencies of QDs.[50, 51]

The shell of QDs structurally separates the photoluminescent core of $CuInSe_2$ from its neighboring environment.[15, 33, 52] All these characteristics can be observed in the schematic representation in (Figure 7). PL intensity and QY of $CuInSe_2$/ZnSe was much higher than that for $CuInSe_2$ [53] core (Figure 6) due to the fact that ZnSe shell growth diminishes the number of surface interactions or bounds, which can develop as trap states for charge carriers and thus reduces the optical properties.[7, 25, 40, 41]

The difference of 1.04 eV between band gap values of $CuInSe_2$ core (1.05 eV) and $CuInSe_2$/ZnSe shell (2.69 eV) can be observed in (Figure 7). It consists of high luminescent chalcopyrite quantum core/shell dots that involves a heterojunction formed by a chalcopyrite p-type photon ($h\nu$) absorber core and for a ($h\nu$) transparent n-type window layer.[54, 55]

Numerous research groups have been investigating the electronic band structures of I-III-VI_2 compounds.[50] Ternary chalcogenides founded Cu element have valence band

maxima with anti-bonding states of Cu-3d orbitals and chalcogens p orbitals and conduction band minima with anti-bonding states generated from III-s orbital and IV-p orbitals. As consequence, ternary Cu-based chalcogenides have smaller band gaps than II-VI compounds due to their display of higher band maxima.[40, 41, 44, 50] Consequently, the electrons in the valence band of ternary chalcogenides such as $CuInSe_2$ can be excited more easily by photons and issue PL radiation, see figure 7.[50]

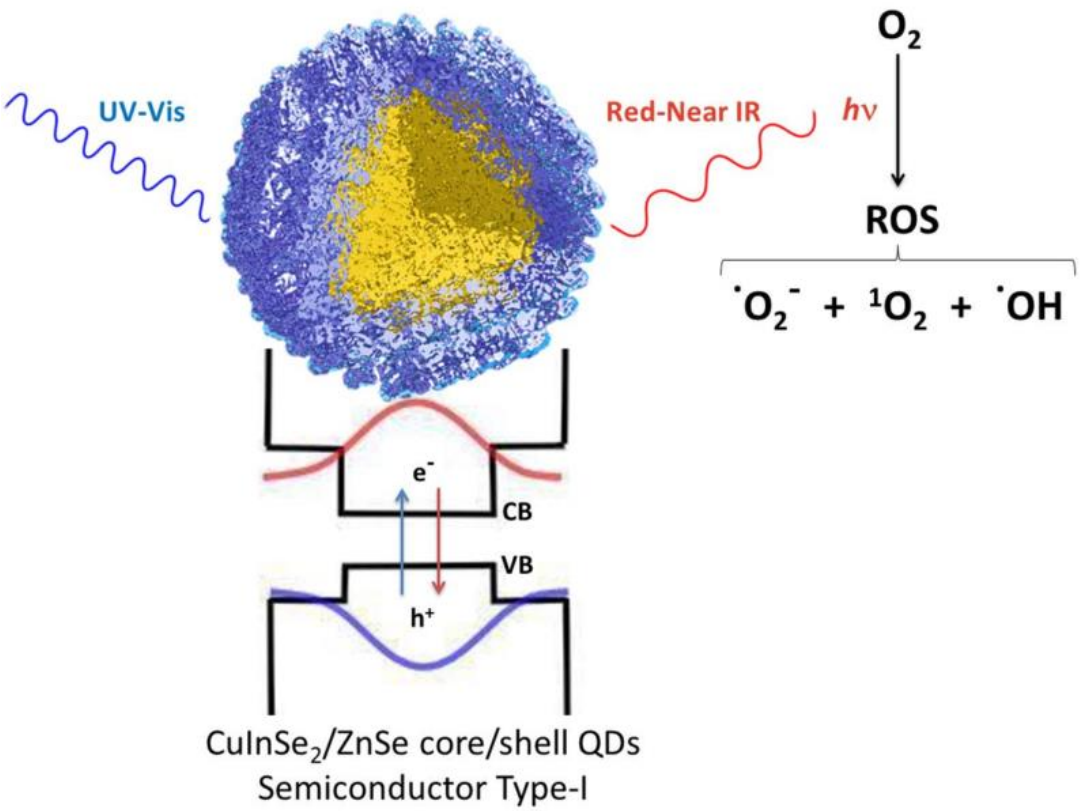

Figure 7. Schematic representation of Pair hole-electron (**h^+-e^-**) localization regime supported by heterostructures of $CuInSe_2$/ZnSe core/shell QDs in the case of a fixed core radius and thin shell widths. Both electron and hole wave functions are localized in the $CuInSe_2$ core. As a result, type I semiconductor $CuInSe_2$/ZnSe core/shell QDs, in which the ZnSe shell is used to passivate the surface of the core with the goal to improve photoluminescence quantum efficiencies of QDs.

Since the core/shell structure is formed by different semiconductor materials, band discontinuities occur at the interface. The calculation of the electron/hole wave function based on spherical potential showed the radial probability distribution of electrons in similar chalcogenide core/shell structures, $CuInS_2$/ZnS, showing highly confined electron wave function.[40, 41] Here we observed in the high increment of fluorescence of $CuInSe_2$/ZnSe core/shell heterostructure over $CuInSe_2$ core. The wave function of each potential region of core/shell structure overlap provided lower chance of hole-electron recombination and increased the life-time of the excited electron-hole. [56]

3.2.4. Near-IR $CuInSe_2$/ZnSe emission, down-converting nanoparticles

$CuInSe_2$/ZnSe core/shell nanoparticles can be defined as down-conversion quantum dots (DC-QD). A DC-QDs are structures that can do scission of photons with energy at double the band gap energy into two lower energy photons, which emit PL in the red, near-IR, and IR regions of electromagnetic spectra. The down-conversion process consists in a transformation, throw a specific material with higher energy of photons into one or more lower energy photons.[57,58] DC properties of this $CuInSe_2$/ZnSe core/shell QDs obtained can be used in converting incident photons with energy larger than an integer multiple of band gap energy of the solar cell material that could be down-converted into a corresponding number of photons with energies larger than the band gap energy.[58] In our interest was to developed a technique to evaluate $CuInSe_2$/ZnSe core/shell nanoparticles as photosensitizer in generation of reactive oxygen species such as singlet oxygen. Considering the dynamics

of energy transformations in this system, we decided it could interesting to evaluate their potential as photosensitizers for the generation reactive oxygen species such as singlet oxygen.[32,35,37,59]

3.2.5. $CuInSe_2$/ZnSe Photosensitizing Properties and singlet oxygen generation

In the past years, an increasing number of studies have been reported, showing that organic and inorganic materials provided photosensitizing environment for generation of singlet oxygen .[3,7,27-32,34,60] A relevant result of our investigation was to probe the photosensitization properties of $CuInSe_2$/ZnSe that involve singlet oxygen ($^1O_2$) production. A reasonably new method for cancer treatment is photodynamic therapy (PDT), which light induced reactive oxygen species production in confined areas and these destroyed malignant tumor cells .[30,32,34] The $CuInSe_2$/ZnSe could be tagged with specific antigen-antibody system, as for assembly of nanostrucutres through streptavidin-biotin interaction [61,62,63], bringing them in close proximity to the tumor cells and administrated systemically. In this context, $CuInSe_2$/ZnSe can act as a kind of photosensitizer drug molecules exhibiting promising application in the PDT for anticancer treatment.[32] $^1O_2$ can be rapidly generated by irradiating $CuInSe_2$/ZnSe core/shell QDs, a reaction mechanism of Type II, which transfers its excited triplet state energy to ground-state oxygen ($^3O_2$).[39,60,64]

DPBF was employed as quencher of $^1O_2$, the fluorescence of DPBF was quenched markedly when it reacted with ^{1}O2; however, it would recover in the presence of a scavenger which could be oxidized by $^1O_2$.[32, 65, 66] The emission spectra of DPBF were recorded and are shown in (figure 8). This figure displays the relative fluorescence intensity

of the system $CuInSe_2$/ZnSe-DPBF in hexane from t_0 (without radiation) to t (with kinetic experiment until 360s).

As can be seen from (figure 8), the relative fluorescence intensity of the system decreased markedly due to the generation of $^1O_2$ by irradiating the $CuInSe_2$/ZnSe-DPBF system with wavelength 400nm.[32,66] This markedly reduced PL intensity with time at intervals of 60s until 360s, when reaction was stopped.

The PL intensity maxima from each interval of time studied was evaluated as a function of time in (figure 8), where its shows decreasing relation. Therefore, knowing $^1O_2$ quenching activity of DPBF, this experiment showed a good capacity of ^{1}O2 production by $CuInSe_2$/ZnSe in the system evaluated.[32, 34, 35, 66] It is emphasized that the DPBF fluorescence without $CuInSe_2$/ZnSe quantum dots samples, themselves was observed at (437-510) nm with excitation at 400nm in our experiments throughout. DPBF reacts with $^1O_2$ suffering a 1,4-cycloaddition, this reaction is determined by a reduction in the PL intensity of the DPBF absorption band above 410nm, as show it in (Figure 9).[34,35,66,67]

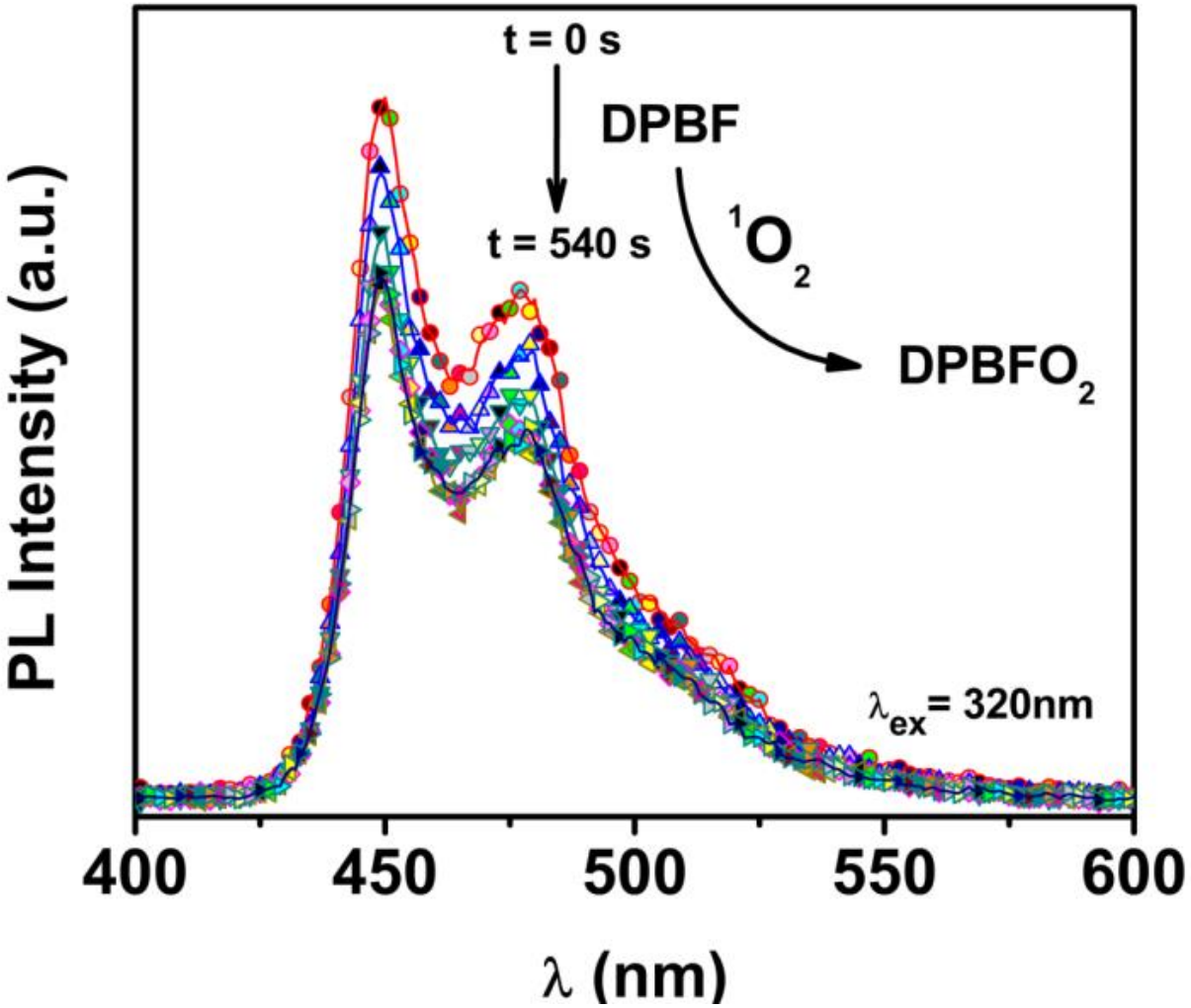

Figure 8. Decay DPBF fluorescence upon reaction of DPBF with singlet oxygen. DPBF was employed as quencher of $^1O_2$, the fluorescence of DPBF was quenched markedly when it reacted with $^1O_2$.The emission spectra of DPBF were recorded and are shown in this figure, where displays the relative fluorescence intensity of the system $CuInSe_2$/ZnSe-DPBF in hexane from t_0 (without radiation) to t (with kinetic experiment until 360s). The relative fluorescence intensity of the system decreased markedly due to the generation of $^1O_2$ by irradiating the $CuInSe_2$/ZnSe-DPBF system with λ=400nm.

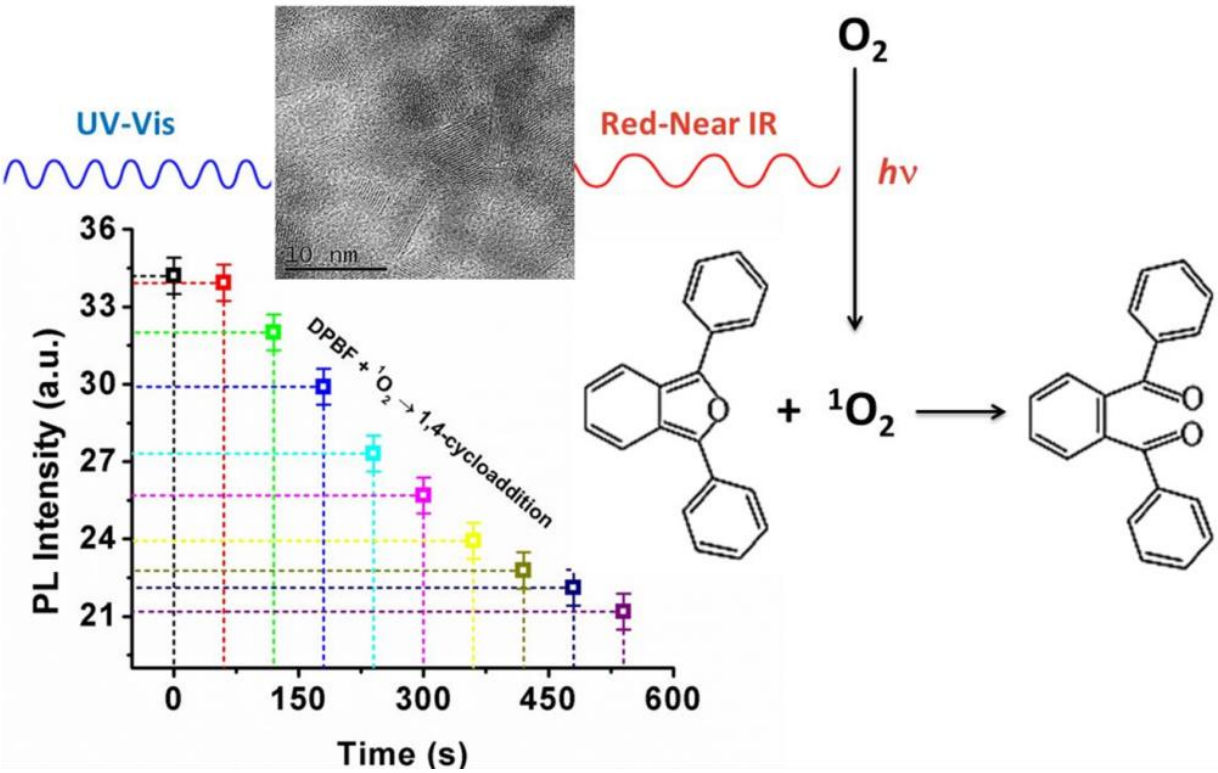

Figure 9. DPBF Kinetic study of the quenching reaction of singlet oxygen. DPBF reacts with $^1O_2$ suffering a 1,4-cycloaddition, that is detected as a decrease in the PL intensity of the DPBF absorption band above 410nm.

As shown in Figure 10, the PL intensity of the solution containing $CuInSe_2$/ZnSe core/shell QDs and DPBF decreases gradually as a function of time under light irradiation, while the change is insignificantly small in the absence of $CuInSe_2$/ZnSe core/shell QDs (figure 11).

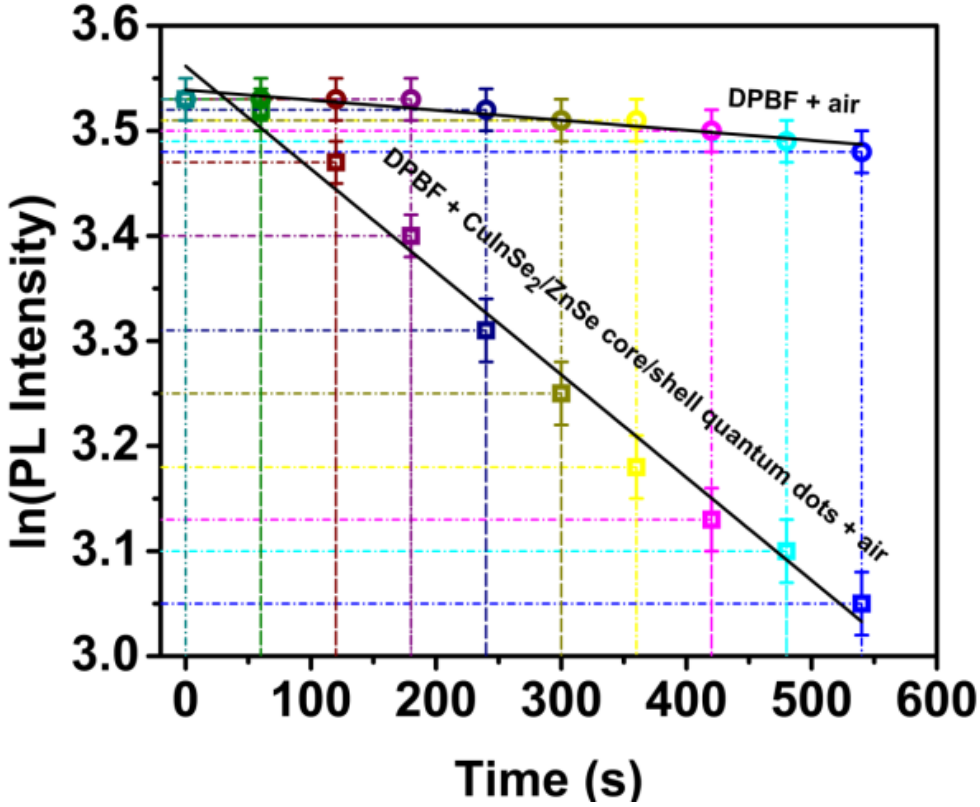

Figure 10. Decay curve in fluorescence intensity of DPBF as a function of irradiation time. DPBF in air and DPBF with $CuInSe_2$/ZnSe core/shell quantum dots in air.

To confirm that the decomposition of DPBF is caused by $^1O_2$ instead of a direct reaction with photo-excited $CuInSe_2$/ZnSe core/shell QDs, the photolysis reaction was carried out in a solution bubble with N_2 to eliminate O_2. The decrease of the PL intensity of DPBF in N_2 bubble QDs suspension was insignificant compared to that of the non-bubble with N_2 QDs suspension (Figure 10). The evolution of the DPBF 1,4-cycloaddition reaction on dissolved O_2 suspension make available strong evidence that $^1O_2$ is generated by the in the photosensitizer activity of the $CuInSe_2$/ZnSe core/shell QDs synthesized.[34,35,66]

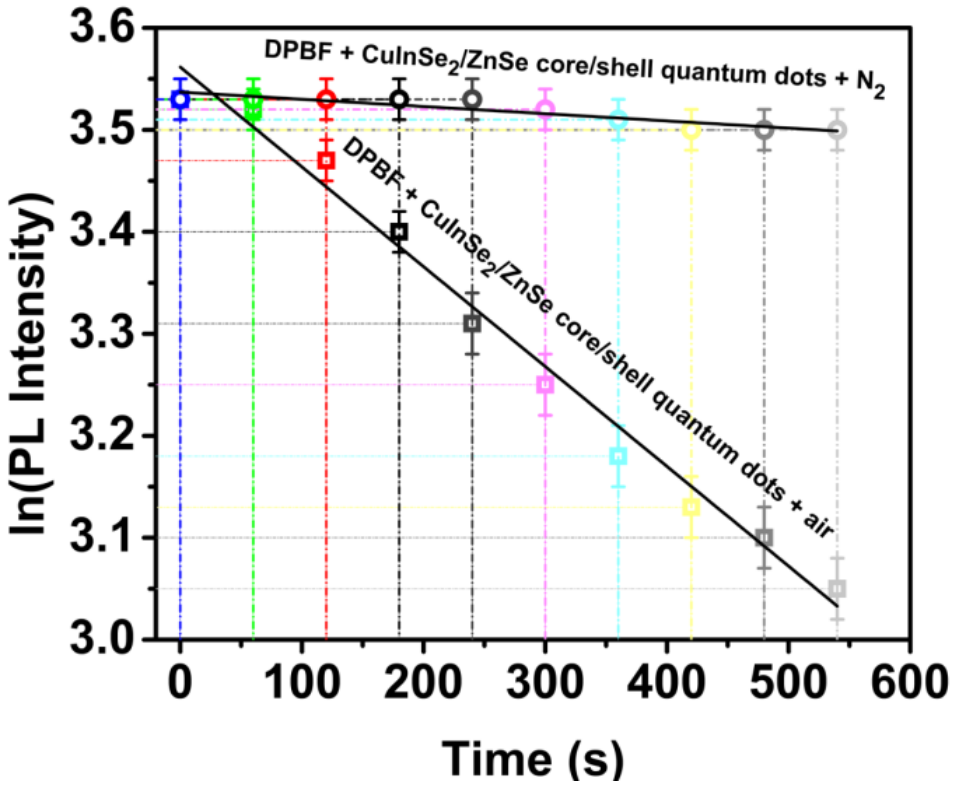

Figure 11. DPBF with $CuInSe_2$/ZnSe core/shell quantum dots in N_2 and DPBF with $CuInSe_2$/ZnSe core/shell quantum dots in air

In recent times, has been exposed generation of $^1O_2$ when quantum-confined areas in porous Si films and nanoparticles are excited with UV-visible light.[34] The energy transfer development is effective due to the vast specific surface area of porous and the exceptionally long lifetime of the excitons of Si films or Si nanoparticles.[34,66,68] A strong photosensitizer with capacity of absorbing and exhausting the energy is necessary to increase energy of oxygen to its singlet state.[37,60,68,] Photosensitizers should exhibit first excited triplet state of appropriate energy value or band gap value (≥95kJ/mol) to permit efficient energy transfer to ground state oxygen according extended Jablonski diagram.[37,69] Although that the singlet oxygen formation energy is 95kJ/mol, which corresponds to the energy of 1270nm, wavelengths longer 800nm are seldom used for PDT due to high

scattering in the tissue and lack of adequate sensitizers that emit PL in near-IR or IR regions.[60] Energies longer 200kJ/mol (~590nm or ~2.1eV) are not desired due in the competition between mechanism type I and II, advantage the first, with more training of ROS than singlet oxygen.[37,69,70] Depend of size of nanoparticle band gap change and the value by quantum confinement and diameter size relationship. The CuInSe2/ZnSe core/shell QDs synthetized have a PL emission optimum energy of 1.546 eV or 154kJ/mol (800nm), as was show it in (Figure 6), to produce singlet oxygen in large quantity that ROS species.[37, 69] Beyond singlet oxygen, QDs produce other reactive oxygen and nitrogen species, previous studies show that electron and/or energy transmission from QDs to adjacent biomolecules accomplished of producing singlet oxygen and other radical species. Recently has been reported studies that support the possibility of using QDs for light induced photo oxidation via both Type II ($^1O_2$ generation) mechanism and Type I (radicals formation).[32,71,72]

For Type II pathway, PDT effect is highly dependent on the oxygen content[70] In cancer therapy, the inner region of a tumor is commonly hypoxic, due to insufficient blood supply .[70,73,74] In addition, oxygen shortages can occur as a result of photochemical consumption and vascular damage during PDT, which further limits efficacy in tumor destructions. The Type I mechanism involves hydrogen-atom abstraction, yielding free radicals. Type I and Type II mechanism can occur simultaneously, even if is supposed that the biological PDT effect id generated by $^1O_2$ formed by Type II mechanism, however, several studies reveal that the ROS from Type I reaction may prime to an improved PDT activity below low oxygen environments.[70] Studies support nanoparticulates systems with capacity to modulate Type I and/or Type II reactions for efficient ROS generation subject

on the tumor cells environment, and $CuInSe_2$/ZnSe core/shell QDs synthetized could be a kind of this tuning o modulator.[32,70,73-75]

It should be emphasized here that $CuInSe_2$/ZnSe core/shell QDs synthetized by this method are very stable on long time maintenance low aggregation a high PL properties through six months, detail in supplementary information (Figure S4A and S4B). Their low solubility is other cumulative value if these are compare with others nanoparticles highly when PDT are applied *in viv*.[32,34]

$CuInSe_2$ and ZnSe are relatively low toxic and their high luminescence, that is produced by the quantum confinement produced by $CuInSe_2$/ZnSe core/shell structure, promote that used very slow quantities of photosensitizer. Additionally known that each photosensitizer of conventional molecular agent can typically produce 10^3-10^5 molecules of $^1O_2$[37], which is a high amount of oxygen species that origin the death of tumor cells.[76] In addition, some authors suggest the combination of PDT with other techniques such as thermolysis.[32,70] $CuInSe_2$/ZnSe core/shell QDs synthetized, when this are irradiated and produced luminescence either produce heat and this combination can improved the results of PDT.[32,70,77,78]

$CuInSe_2$/ZnSe core/shell QDs can applied in treatment of cancer by local hyperthermia with only change energy of irradiation to move PL emission to more near-IR and/or IR .[77,78,79] On the other hand, physicochemical properties of $CuInSe_2$/ZnSe core/shell QDs synthetized can provide a safe and environmentally benign nanomaterial with antibacterial properties, by tuning $^1O_2$ and others ROS production, with variation in composition, size, and/or wavelength on irradiation energy.[80]

3.2.6. Partial conclusions for $CuInSe_2$/ZnSe core/shell QDs system

1. A novel and sustainable way to synthesize high fluorescence $CuInSe_2$ core and $CuInSe_2$/ZnSe core/shell QDs has been developed
2. $CuInSe_2$/ZnSe core/shell QDs with nearly stoichiometric composition and excellent PL properties were synthetized.
3. Quantum confinement effects were observed at 800nm, for red and Near-IR emission, for excitonic transitions in the $CuInSe_2$ QDs, as predicted by their small diameter of approximately 4nm, and 6 nm to $CuInSe_2$/ZnSe core/shell QDs, related to the 10.6nm of the bulk exciton Bohr radius.
4. The PL QYs of $CuInSe_2$/ZnSe core/shell QDs increased from 11% to 62%, with respect to $CuInSe_2$ core emission.
5. The preliminary results demonstrated the potential of $CuInSe_2$ core and $CuInSe_2$/ZnSe core/shell nanoparticles with comparatively low toxicity to different materials for the advanced development of extensive optical device application as photosensitizer in ROS production.
6. $CuInSe_2$/ZnSe core/shell QDs nanoparticle as photosensitizer was evaluated by kinetic study were performed on the singlet oxygen quenching reaction with DPBF, which is promising in application as photodynamic therapy and solar cells.

3.3. Future developments: $CuInSe_2$ QDs – PVA thin films structures for inorganic - organic hybrid solar cell

3.3.1. Abstract

$CuInSe_2$ quantum dots semiconductor chalcogenide nanocrystals were synthesized by an organometallic method by the reaction of copper and indium salts with various sulfur and selenium sources, tri-n-octylphosphine, and oleylamine in octadecene solvent, with a moderate reaction temperature (240°C). The structural and optoelectronic characterization of the soot produced in the reaction was investigated through X-ray diffraction (XRD) and Photoluminescence. XRD a chalcopyrite type structure with crystallite size of about 4 nm. The as-prepared quantum dots nanocrystals exhibit photoluminescence in the range of 600-900 nm. This particles was used to prepare an inorganic-organic hybrid for solar cell by QDs-PVA composite thin films.

3.3.2. Introduction

Fluorescent organic and inorganic materials are promising in studying the complexity and dynamics of biological process [1,2]. The physicochemical properties will change radically as the materials evolve from the bulk level to the atomic or molecular counterparts [3]. Compared to the traditional dyes (fluorescent organic molecules), semiconductive nanocrystals have broader excitation wavelength range, narrower and tunable emission spectra [1], more resistant to chemicals and metabolic degradation, and higher photobleaching threshold. In this work, a transparent poly (vinyl alcohol) (PVA) nanocomposite thin film (30–50 nm) reinforced with core/shell $CuInSe_2$ quantum dots (QDs) was fabricated by a spin coating method. A narrow peak at 800nm observed in the

UV–vis spectrum indicates the uniformly dispersed QDs in the PVA matrix. FT-IR analysis indicates the interaction between the QDs and the polymer matrix. Both PVA and PVA-QDs nanocomposite thin films show polarized light dependent absorption properties with several different absorption peaks. As compared to the only fluorescent emission peak at 800nm of QDs, the pure PVA and PVA-DDs nanocomposites show an excitation wavelength dependent fluorescent emission property.

3.3.3. Experimental methods

3.3.3.1. QDs synthesis

3.3.3.1.1. Chemicals:

Copper(I) acetate (CuA 98%), Indium(III) acetate ($In(OAc)_3$, 99.99%) from Acros Organics. oleylamine (OA, 90%), 1-dodecanethiol (DDT, 97%), 1-octadecene (ODE, 90%), acetone and methanol from Sigma-Aldrich. Zinc acetate (90%) dehydrate, sodium diethyldithiocarbamate trihydrate (97%) from Alfa Aesar. Poly(Vinyl Alcohol) (PVA) 99% from Alfa Aesar.

3.3.3.1.2. General procedure

Values in brackets indicate quantities of material. $In(OAc)_3$ (1.44 g) and CuA (0.586 g) were mixed with 0.1mmol of selenourea for Se configurations and 25 mL of ODE in a 100 mL three-neck flask under an inert atmosphere. The mixture was heated to reaction temperature at 240 °C under primary vacuum and stirring for 30 min. The color of the reaction solution progressively changed from colorless, yellow, orange, red, deep red and finally dark brown. The mixture was kept at reaction temperature for 30 min. While waiting for synthesis the ZnS precursor was made by mixing 0.1mol of selenourea for Se structures and 20 ml of OA. After core being 30 min in reaction temperature, 20 ml of ZnS (or ZnSe)

precursor were added drop wise by syringe pump. The mixture was removed from heating source and isolated by adding abundant methanol. For precipitating acetone was added followed by centrifuging. The precipitation/dispersion cycle was repeated at three times in order to eliminate byproducts. ZnDDTC for ZnSe precursor was prepared by a precipitation reaction under ambient condition. 4.4 g zinc acetate dehydrate was dissolved in 200 mL of distilled water in a 500 mL beaker. 9.0 g of sodium diethyldithiocarbamate was dissolved in 80 mL of distilled water and added dropwise into zinc acetate solution with vigorous stirring. The mixture was kept stirring for 30 min after the addition. The resulting white precipitates were filtered, washed with distilled water, and dried under vacuum at 50 °C.

3.3.3.1.3. PVA film preparation

All of the films produced were made from a 15% aqueous PVA solution. To prepare the PVA solution, 30 ml of deionized water was added to 5.3 g PVA (Elvanol 90-50; Mn = 37740, degree of hydrolysis = 99%, polydispersity index = 2.15, E.I. DuPont de Nemours & Co., Wilmington, DE, United States). The PVA solution was heated at 90°C for 4 to 6 h. The solution was allowed to cool for several minutes before use. The solution was then cast onto six 75 x 50 mm SiO_2 slides and spread uniformly over the slides using a glass rod. The films were allowed to dry at 25°C for at least 24 h. The amorphous PVA films were then annealed in an oven for times ranging from 15 to 90 min at temperatures of 90 to 120°C. Once the films were removed from the oven, they were peeled off of the glass slides and stored at room temperature.

3.3.3.1.4. PVA-QDs nanocomposite thin film fabrication

3 g quantum dots per 100 g solution was added into PVA aqueous solution. The PVA-QDs nanocomposite thin film was made following the same procedures as those used for the pure PVA thin film fabrication by Spin Coating techniques.

The typical film thickness was measured to be 15 to 20 layers of $CuInSe_2$ and PVA.

3.3.3.1.5. Characterization

The structural and optoelectronic characterization of the soot produced in the reaction was investigated through X-ray diffraction analysis and photoluminescence measurement.

3.3.4. Results

Here we show preliminary results about structural and optical properties.Structural Characterization: The structural phases of CuInSe2 were acquired by means of X-ray diffraction (XRD) characterizations. (Figure 1) shows the XRD patterns of the $CuInSe_2$ quantum dots nanoparticles synthesized and $CuInSe_2$ QDs – PVA composite. The diffraction peaks can be indexed to the (112), (204)/(220), and (116)/(312) reflections of the tetragonal crystal structure of $CuInSe_2$ chalcopyrite phase. The absence of diffraction peak of (200), distinguishing peak of zincblende phases, enables us to excluded the development of the CuInSe2 zincblende phase. After the sample was coated with the PVA, all peaks exhibited the same angles. The Scherrer equation was used to determine the size of CuInSe2 core and CuInSe2/ZnSe core/shell QDs, the average diameters calculated were 3.6nm and 5.5nm, respectively, with ±0.5nm of error. We used the Scherrer constant of 0.89 for tetrahedral structures perpendicular to the plane (111) in cubic phase, due this equals to (112) plane of tetragonal phase.

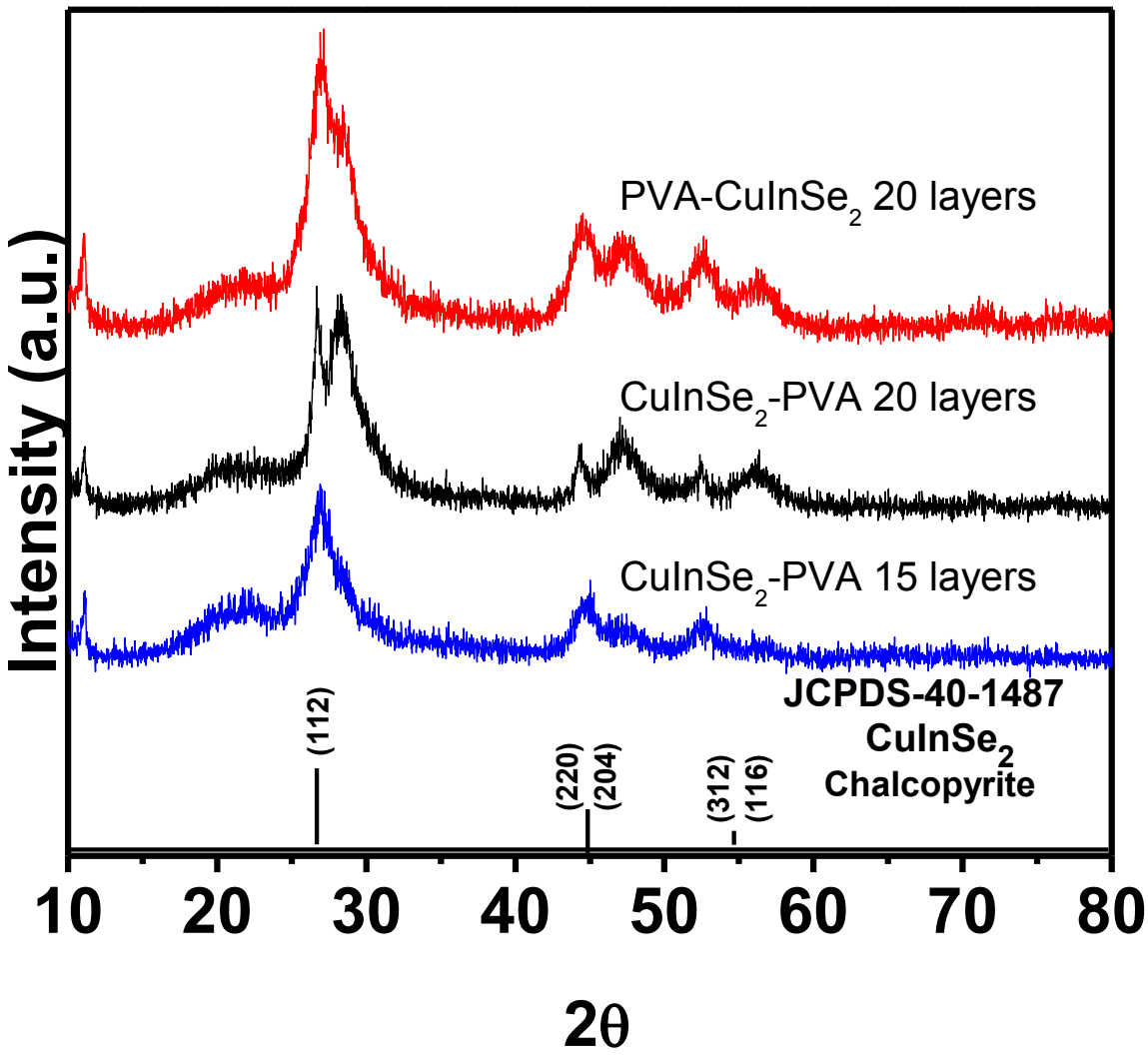

Figure 12. XRD patterns of $CuInSe_2$ – PVA QDs systems

Optical characterization: Figure 2 shows the fluorescence spectra of QDs aqueous solution, pure PVA thin film and PVA-QD nanocomposite thin film, respectively. The excitation wavelength was 350 nm. A peak at 800nm was observed in both QDs aqueous solution and PVA-QD nanocomposite thin film, which was characteristic of CuInSe2 quantum dots. No fluorescence phenomenon was observed in pure PVA thin film in the observed wavelength ranging from 400nm to 900nm.

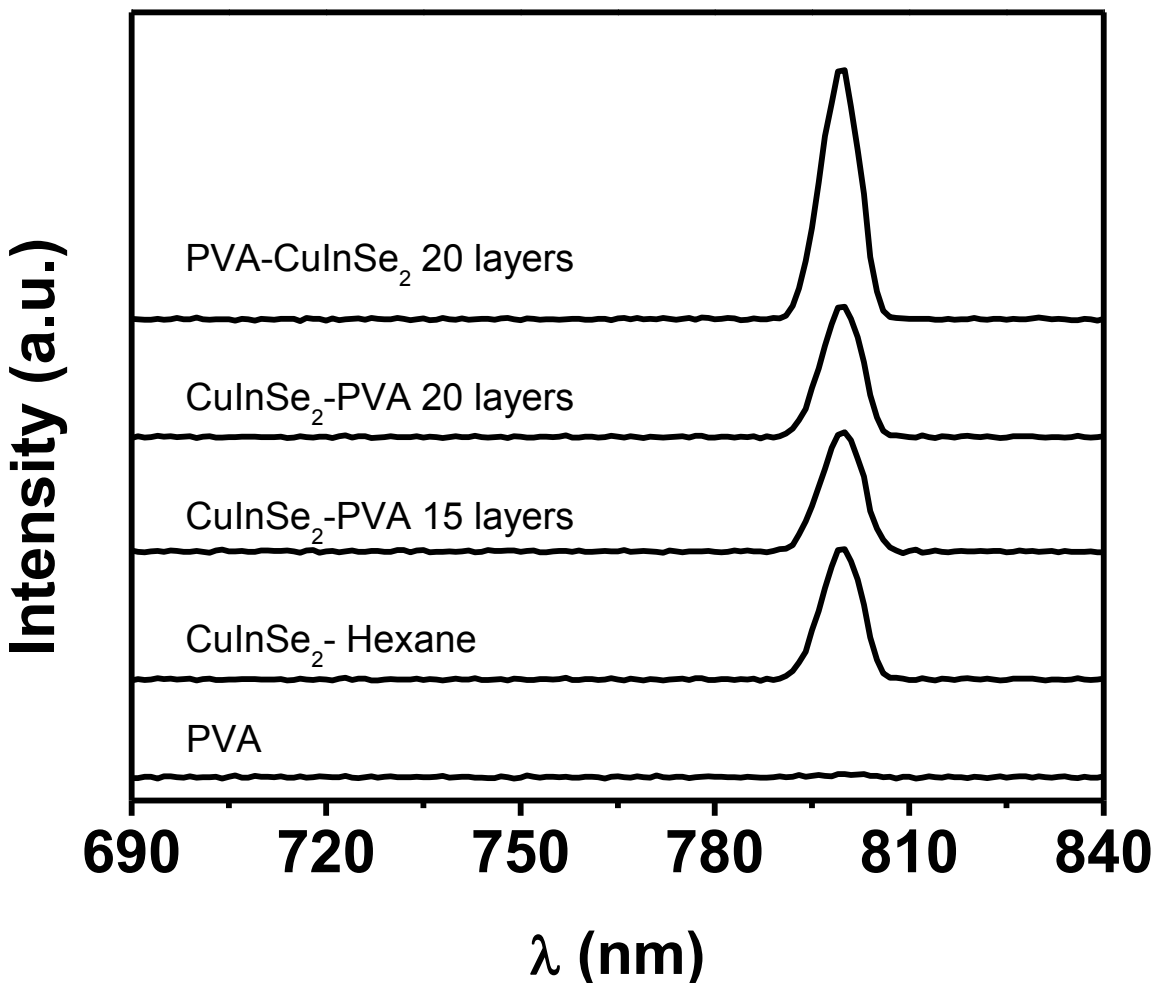

Figure 13. PL spectra of PVA, $CuInSe_2$ QDs in hexane and PVA-$CuInSe_2$ systems

3.3.5. Partial conclusions for $CuInSe_2$ QDs-PVA thin films

$CuInSe_2$ quantum dots were used to prepare PVA-QDs nanocomposite method. With the aid of UV–vis spectrophotometer, the polymer composites showed absorption at 400 nm, similar to the pure QDs solution. The nanocomposites showed a PL emission of the polymer and the nanosized fillers. The composites have also shown special optical absorption property when subjected to polarized beams in PL test. During fluorescence test, a stable emission peak for QDs and a shifting peak for PVA were observed. With

transparent biodegradable PVA as base material, nanocomposites reinforced with QDs have great potential optical electronic applications. With the fluorescent quantum dots as nanofillers, these nanocomposites have great potential applications in the solar cell area.

3.3.6. Partial references for $CuInSe_2$ QDs-PVA thin films

1. J. H. Kim, J. Y. Jin, J. H. Jung, I. Lee, T. W. Kim, S. K. Lim, C. S. Yoon and Y. H. Kim "Formation and electrical properties of Ni1-xFex nanocrystals embedded in a polyimide layers for applications as nonvolatile flash memories". *Appl. Phys. Lett.*, Vol. 86, No. 3, pp 032904-1 - 032904-3, 2005.

2. F. Li, D. I. Son, J. H. Ham, G. J. Kim, J. H. Jung and T. W. Kim "Memory effect of nonvolatile bistable devices based on CdSe/ZnS nanoparticles sandwiched between C60 layers". *Appl. Phys. Lett.*, Vol. 91, No. 16, pp 162109-1 - 162109-3, 2007.

3. K. Mohanta, S. Majee, S. Batabyal and A. Pal "Electrical bistability in electrostatic assemblies of CdSe nanoparticles". *J. Am. Chem. Soc.*, Vol. 110, No. 37, pp 18231-18235, 2006.

4. CONCLUSIONS

In summary, high fluorescence $CuInS_2$ and $CuInSe_2$ core and $CuInS_2$/ZnS and$CuInSe_2$/ZnSe core/shell QDs, respectively, has been synthetized. Specifically, a novel and sustainable way to synthesize CuInSe2 and CuInSe2/ZnSe QDs was developed. This technique can produce $CuInSe_2$/ZnSe core/shell QDs with nearly stoichiometric composition and excellent PL properties. Quantum confinement effects were observed at (700-850) nm region, for red and Near-IR emission, for excitonic transitions in the $CuInS_2$ and $CuInSe_2$ QDs, as predicted by their small diameter of approximately 5nm and 4nm, respectively, related to the 10.6nm of the bulk exciton Bohr radius. Equivalent effect was observed around 6 nm to $CuInS_2$/ZnS and $CuInSe_2$/ZnSe core/shell QDs.

The PL QYs of $CuInSe_2$/ZnSe, and $CuInSe_2$/ZnSe, core/shell QDs increased from, 9% to 47%, and 11% to 62%, with respect to $CuInS_2$, and $CuInSe_2$, core emission respectively. The preliminary results demonstrated the potential of $CuInSe_2$ core and $CuInSe_2$/ZnSe core/shell nanoparticles with comparatively low toxicity to different materials, such as $CuInS_2$/ZnS system, for the advanced development of extensive optical device application as photosensitizer in ROS production, as well as biosensors or bioimaging, centered on the conjugation of these heterostrucrures Type-I to biological units.

$CuInSe_2$/ZnSe core/shell QDs nanoparticle as photosensitizer was evaluated by kinetic study were performed on the singlet oxygen quenching reaction with DPBF, which is promising in application as photodynamic therapy and solar cells.

5. REFERENCES

1. Alivisatos, A. P. Perspectives on the Physical Chemistry of Semiconductor Nanocrystals. *J. Phys. Chem.* **1996**, *100 (31)*, 13226-13239.
2. Murray, C. B.; Kagan, C. R.; Bawendi, M. G. Synthesis and Characterization of Monodisperse Nanocrystals and Close-Pacjked Nanocrystals Assemblies. *Annu. Re*v. *Mater. Sci.* **2000**, *30*, 545-610.
3. Niemeyer, C. M. Nanoparticles, Proteins, and Nucleic Acids: Biotechnology Meets Materials Science. *Angew. Chem. Int. Ed.* **2001**, *40*, 4128-4158.
4. Chan, W. C. W.; Nie, S. Quantum Dot Bioconjugates for Ultrasensitive Nonisotopic Detection. *Science*. **1998**, *281 (5385)*, 2016-2016.
5. Bruchez, M. J.; Moronne, M.; Gin, P.; Weiss, S.; Alivisatos, A. P. Semiconductor nanocrystals as fluorescent biological labels. *Science*. **1998**, *281 (5385)*, 2013-2016.
6. Liu, X.; Jiang, Y.; Lan, X.; Zhang, Y.; Li, S.; Li, J.; Han, T.; Wang, B.; Zhong, H. Highly luminescent blue emitting CdS/ZnS core/shell quantum dots via a single-molecular precursor for shell growth. *Materials Chemistry and Physics*. **2011**, *130 (3)*, 909– 914.
7. Reiss, P.; Protière, M.; Li, L. Core/Shell Semiconductor Nanocrystals. *Small*. **2009**, *5 (2)*, 154–168.
8. Gur, I.; Fromer, N. A.; Geier, M. L.; Alivisatos, A. P. Air-Stable All-Inorganic Nanocrystal Solar Cells Processed from Solution. *Science*. **2005**, *310 (5747)*, 462-465.
9. Kumar, S.; Scholes, G. D. Colloidal Nanocrystal Sollar Cells. *Microchim.* Acta. **2008**, *160*, 315-325.

10. Rogach, A. L.; Gaponik, N.; Lupton, J. M.; Bertoni, C.; Gallardo, D. E.; Dunn, S.; Pira, N. L.; Paderi, M.; Repetto, P.; Romanov, S. G.; O'Dwyer, C.; Torres, C. M. S.; Eychmu¨ller, A. *Angew.* Light-emitting Diodes with Semiconductor Nanocrystals. *Chem. Int. Ed. Engl.* **2008**, *47(35)*, 6538-6549.
11. Huynh, W. U.; Dittmer, J. J.; Alivisatos, A. P. Hybrid Nanorod-Polymer Solar Cells. *Science*. **2002**, *295 (5564)*, 2425-2427.
12. Peng, X. An Essay on Synthetic Chemistry of Colloidal Nanocrystals. *Nano Res.* **2009**, *2*, 425-447.
13. Zhong, H.; Zhou, Y.; Ye, M.; He, Y.; Ye, J.; He, C.; Yang, C.; Li, Y. Controlled Synthesis and Optical Properties of Colloidal Ternary Chalcogenide $CuInS_2$ Nanocrystals. *Chem. Mater.* **2008**, *20 (20)*, 6434-6443.
14. Krunks, M.; Bijakina, O.; Varema, T.; Mikli, V.; Mellikov, E. Structural and Optical Properties of Sprayed $CuInS_2$ films. *Thin Solid Films*. **1999**, *338 (1)*, 125-130.
15. Xie, R.; Rutherford, M.; Peng, X. J. Formation of High-Quality I-III-VI Semiconductor Nanocrystals by Tuning Reactivity of Cationic Precursors. *Am. Chem. Soc.* **2009**, *131 (15)*, 5691-5697.
16. Haus, J.W.; Zhou, H.S.; Honma, I.; Komiyama, H. Quantum Confinement in Semiconductor Heterostructure nanometer-size particles. *Phys. Rev. B Condens Matter*. **1993**, *47 (3)*, 1359-1365.
17. Omata, T.; Nose, K.; Otsuka-Yao-Matsuo, S. Size Dependent Optical Band Gap of Ternary I-III-VI_2 Semiconductor Nanocrystals. *J. Appl. Phys*. **2009**, *105*, 0731061-0731066.

18. Ganther, H.E. Selenium metabolism, selenoproteins, and mechanisms of cancer prention: complexities with thioredoxin reductase. *Carcinogenesis*. **1999**, *20 (9)*, 1657-1666.

19. Guénaud, C.; Deleporte, E.; Filoramo, A.; Lelong, P.; Delalande, C.; Morhain, C.; Tournié, E.; Faurie, J.-P. Study of the Band Alignment in (Zn,Cd)Se/ZnSe Quantum Wells by Means of Photoluminescence Excitation Spectroscopy. *J. Appl. Phys.* **2000**, 87, 1863-1868.

20. Reiss, P.; Bleuse, J.; Pron, A. Highly Luminescent CdSe/ZnSe Core/Shell Nanocrystals of Low Size Dispersion. *Nano Lett.* **2002**, *2(7)*, 781-784.

21. Reiss, P. ZnSe based Colloidal Nanocrystals: Synthesis, Shape Control, Core/Shell, Alloy and Doped Systems. *New. J. Chem.* **2007**, *31*, 1843-1852.

22. Li, L.S.; Pradhan, N.; Wang, Y.; Peng, X. High Quality ZnSe and ZnS Nanocrystals Formed by Activating Zinc Carboxylate Precursors. *Nano Lett.* **2004**, *4 (11)*, 2261-2264.

23. Reiss, P.; Carayon, S.; Bleuse, J.; Pron, A. Low Polydispersity Core/Shell Nanocrystals of CdSe/ZnSe and CdSe/ZnSe/ZnS type: preparation and optical studies. *Synthetic Metals*, **2003**, *139*, 649-652.

24. Corrado, C.; Hawker, M.; Livingston, G.; Medling, S.; Bridges, F.; Zhang, J.Z. Enhanced Cu Emission in ZnS: Cu,Cl/ZnS Core-Shell Nanocrystals. *Nanoscale*. **2010**, *2*, 1213-1221.

25. Lee, J.; Han, C.-S. Large-Scale Synthesis of Highly Emissive and Photostable $CuInS_2$/ZnS Nanocrystals Through hybrid flow reactor. *Nanoscale Research Letters*. **2014**, *9 (78)*, 1-8.

26. Xu, J.; Lee, C.-S.; Tang, Y.-B.; Chen, X.; Chen, Z.-H.; Zhang, W.-J.; Lee, S.-T.; Zhang, W.; Yang, Z. Large-Sacale Synthesis and Phase Transformation of CuSe, $CuInSe_2$, and $CuInSe_2/CuInS_2$ Core/Shell Nanowire Bundles. *ACS Nano*. **2010**, *4 (4)*, 1845-1850.
27. Fang, M.; Peng, C.-W.; Pang, D.-W.; Li, Y. Quantum Dots for Cancer Research: Current Status, Remaining Issues, and Future Perspectives. *Cancer Biol. Med.* **2012**, *9*, 151-163.
28. Pisanic Il, T.R.; Zhang, Y.; Wang, T.H. Quantum Dots in Diagnostics and Detection: Principles and paradigms. *Analyst.* **2014**, *139*, 2968-2981.
29. MacCormack, M.A. Photodynamic Therapy in Dermatology: An Update on Applications and Outcomes. *Semin. Cutan. Med. Surg.* **2008**, *27*, 52-62.
30. Samia, A.C.S.; Dayal, S.; Burda, C. Quantum Dot-based Energy Transfer: Perspectives and Potential for Applications in Photodynamic Therapy. *Photochemistry and Photobiology*. **2006**, *82*, 617-625.
31. Bera, D.; Qian, L.; Tseng, T.-K.; Holloway, Paul H. Quantum Dots and Their Multimodal Applications: A Review. *Materials*. **2010**, *3*, 2260-2345.
32. Juzenas, P.; Chen, W.; Sun, Y.-P.; Neto Coelho, M.A.; Generalova, R.; Generalova, N.; Lie Chrisyensen, I. Quantum Dots and Nanoparticles for Photodynamic and Radiation therapies of cancer. *Advanced Drug Delivery Reviews*. **2008**, *60*, 1600-1614.
33. Ivanov, S.A.; Piryatinsky, A.; Nanda, J.; Tretiak, S.; Zavadil, K.R.; Wallace, W.O.; Werder, D.; Klimov, V.I. Type-II Core/Shell CdS/ZnSe Nanocrystals: Synthesis, Electronic Structures, and Spectroscopic Properties. *J. Am. Chem. Soc.* **2007**, *129*, 11708-11719.

34. Xiao, L.; Gu, L.; Howell, S.B.; Sailor, M.J. Porous Silicon Nanoparticle Photosensitizers for Singlet Oxygen and Their Phototoxicity against Cancer Cells. *ACS Nano*. **2011**, *5 (5)*, 3651-3659.

35. Howard, J.A.; Mendenhall, G.D. Autoxidation and Photooxidation of 1,3-Diphenylisobenzofuran: A Kinetic and Product Study. *Can. J. Chem.* **1975**, *53*, 2199-2201.

36. Mukai, K.; Ouchi, A.; Nakano, M. Kinetic Study of the Quenching Reaction of Singlet Oxygen by Pyrroloquinolinequinol (PQQH2, a Reduced Form of Pyrroloquinolinequinone) in Micellar Solution. *J. Agric. Food Chem.* **2011**, *59*, 1705-1712.

37. DeRosa, M.C.; Crutchley, R.J. Photosensitized Singlet Oxygen and Its Applications. *Coord. Chem. Rev.* **2002**, *233-234*, 351-371.

38. Ohyashiki, T.; Nunomura, M.; Katoh, T. Detection of superoxide anion radical in phospholipid liposomal membrane by fluorescence quenching method using 1,3-diphenylisobenzofuran. *Biochimica et Biophysica Acta*. **1990**, *1421*, 131-139.

39. Pospísil, P. Molecular mechanisms of production and scavenging of reactive oxygen species by photosystem II. *Biochimica et Biophysica Acta*. **2012**, *1817*, 218-231.

40. Li, L.; Daou, T.J.; Texier, I.; Kim Chi, T.T.; Quang Lien, N.; Reiss, P. Highly Luminescent $CuInS_2$/ZnS Core/Shell Nanocrystals: Cadmium-Free Quantum Dots for in vivo Imaging. *Chem. Mater.* **2009**, *21*, 2422-2429.

41. Deng, D.; Chen, Y.; Cao, J. Tian, J. Qian, Z.; Achilefu, S.; Gu, Y. High-Quality $CuInS_2$/ZnS Quantum Dots for In vitro and In vivo Bioimaging. *Chem. Mater.***2012**, *24*, 3029-3037.

42. Langford, J.I.; Wilson, A.J.C. Scherrer after 60 Years - Survey and Some New Results in Determination of Crystallite Size. *J. Appl. Crystallogr*. **1978**, *11*, 102–113.

43. Zhong, H.; Lo, S.S.; Mirkovic, T.; Li, Y.; Ding, Y.; Li, Y.; Scholes, G.D. Noninjection Gram-Scale Synthesis of Monodisperse Pyramidal $CuInS_2$ Nanocrystals and Their Size-Dependent Properties. *ACS Nano*. **2010**, *4 (9)*, 5253-5262.

44. Koo, B.; Patel, R. N.; Korgel, B. A. Synthesis of $CuInSe_2$ Nanocrystals with Trigonal Pyramidal Shape. *J. Am. Chem. Soc.* **2009**, *131*, 3134–3135.

45. Morphology effects in nanocrystalline $CuInSe_2$-conjugated polymer hybrid systems. *Appl. Phys. A*. **2004**, *79*, 59-64.

46. Zhong, H.; Wang, Z.; Bovero, E.; Lu, Z.; van Veggel, F.C.J.M.; Scholes, G.D. Colloidal CuInSe2 Nanocrystals in the Quantum Confinement Regime: Synthesis, Optical Properties, and Electroluminescence. *J. Phys. Chem. C.* **2011**, *115*, 12396–12402.

47. Chen, H.; Yu, S.-M.; Shin, D.-W.; Yoo, J.-B. Solvothermal Synthesis and Characterization of Chalcopyrite $CuInSe_2$ Nanoparticles. *Nanoscale Res. Lett.* **2010**, *5*, 217-223.

48. Kashyout, A.E-H.B.; Ahmed, E.-Z.; Meaz, T.; Nabil, M.; Amer, M. (One-step) electrochemical deposition and characterization of $CuInSe_2$ thin films.

Alexandria Eng. J. **2014**, , http://dx.doi.org/10.1016/j.aej.2014.03.015 (in press).

49. Saikia, K.; Deb, P.; Kalita, E. Sensitive fluorescence response of ZnSe(S) quantum dots: an efficient fluorescence probe. *Phys.Scr.* **2013**, *87*, 065802.
50. Fan, F.-J.; Wu, L.; Yu, S.-H. Energetic I–III–VI_2 and I_2–II–IV–VI_4 Nanocrystals Synthesis, Photovoltaic and Thermoelectric Applications. *Energy Environ. Sci.* **2014**, *7*, 190-208.
51. Balet, L.P.; Ivanov, S.A.; Piryatinski, A.; Achermann, M.; Klimov, V.I. Inverted Core/Shell Nanocrystals Continuously Tunable between Type-I and Type-II Localization Regimes. **2004**, *4 (8)*, 1485-1488.
52. O'Connor, T.; Panov, M.S.; Mereshchenko, A.; Tarnovsky, A.N.; Lorek, R.; Perera, D.; Diederich, G.; Lambright, S.; Moroz, P.; Zamkov, M.. The Effect of the Charge-Separating Interface on Exciton Dynamics in Photocatalytic Colloidal Heteronanocrystals. *ACS Nano.* **2012**, *6 (9)*, 8156-8165.
53. Amit, S.; Dashora, A.; Gupta, V.; Arora, C.M.; Rérat, M.; Ahuja, B.L.; Pandey, R. Electronic and Optical Modeling of Solar Cell Compounds $CuGaSe_2$ and $CuInSe_2$. *Journal of Elec. Materi.* **2011**, *40*, 2197-2208.
54. Niemegeers, A.; Burgelman, M.; De Vos, A. On the CdS/CuInSe2 conduction band discontinuity. *Appl. Phys. Lett.* **1995**, *67 (6)*, 843-845.
55. Schooss, D.; Mews, A.; Eychmüller, A.; Weller, H. Quantum-dot quantum well CdS/HgS/CdS: Theory and Experiment. *Phys. Rev. B.* **1994**, *49 (24)*, 17072-17078.

56. Kim, Y.-K.; Ahn, S.-H.; Choi, G.-C.; Chung, K.; Cho, Y.-S.; Choi, C.-J. Photoluminescence of CuInS2/(Cd,Zn)S Nanocrystals as aFunction of Shell Composition. *Trans. Electr. Electron. Mater.* **2011**, *12 (5)*, 218-221.

57. Trupke, T.; Green, M.A.; Würfel, P. Improving solar cell efficiencies by up-conversion of sub-band-gap light. *J. Appl. Phys.* **2002**, *92*, 1968-1674.

58. Solar energy enhancement using down-converting particles: A rigorous approach. *J. Appl. Phys.* **2011**, *109*, 1149051-1149059.

59. Jockush, S.; Sivaguru, J.; Turro, N.J.; Ramamurthy, V. Direct measurement of the singlet oxygen lifetime in zeolites by near-IR phosphorescence. *Photochem. Photobiol. Sci.* **2005**, *4*, 403-405.

60. Marmo Moreira, L.; Vieira dos Santos, F.; Pereira Lyon, J.; Maftoum-Costa, M.; Pacheco-Soares, C.; Soares da Silva, N. Photodynamic Therapy: Porphyrins and Phthalocyanines as Photosensitizers. *Aust. J. Chem.* **2008**, *61*, 741–754.

61. Eskelinen, A.-P.; Kuzyk, A.; Kaltiaisenaho, T.K.; Timmermans, M.Y.; Nasibulin, A.G.; Kauppinen, E.I.; Törmä, P. Assembly of Single-Walled Carbon Nanotubes on DNA-Origami Templates through Streptavidin–Biotin Interaction. *Small*. **2011**, *7 (6)*, 746-750.

62. Thermal ablation of tumor cells with antibody-functionalized single-walled carbon nanotubes. *PNAS*. **2008**, *105 (25)*, 8697-8702.

63. Zhou, X.; Moran-Mirabal, J.M.; Craighead, H.G.; McEuen, P. Supported lipid bilayer/carbon nanotube hybrids. *Nature Nanotechnology*. **2007**, *2*, 185-190.

64. Wilkinson, F.; Helman, W.P.; Ross, A.B. Quantum Yields for the Photosensitized Formation of the Lowest Electronically Excited Singlet State of Molecular Oxygen in Solution. *J. Phys. Chem. Ref.* Data. **1993**, *22*, 113-262.

65. He, X.; Wu, X.; Wang, K.; Shi, B.; Hai, L. Methylene blue-encapsulated phosphonate-terminated silica nanoparticles for simultaneous in vivo imaging and photodynamic therapy. *Biomaterials*. **2009**, *30*, 5601-5609.

66. Fuji, M.; Usui, M.; Hayashi,S.; Gross, E.; Kovalev, D.; Krunzner, N.; Diener, J.; Timoshenko, V.Y. Chemical Reaction Mediated by Excited States of Si Nanocrystals – Singlet Oxygen Formation in Solution. *J. Appl. Phys.* **2004**, *95 (7)*, 3689-3693.

67. Laing, M. The Three Forms of Molecular Oxygen. *J. Chem. Educ.* **1989**, *66 (6)*, 453-455.

68. Kovalev, D.; Fujii, M. Silicon Nanocrystals: Photosensitizer for Oxygen Molecules. *Adv. Mater.* **2005**, 17, 2531–2544.

69. Bonnett, R. Photosensitizers of the porphyrin and phthalocyanine series for photodynamic therapy. *Chem. Soc. Rev.* **1995**, *24*, 19-33.

70. Ding, H.; Yu, H.; Dong, Y.; Tian, R.; Huang, G.; Boothman, D.A.; Sumer, B.D.; Gao, J. Photoactivation switch from type II to type I reactions by electron-rich micelles for improved photodynamic therapy of cancer cells under hypoxia. *Journal of Controlled Release.* **2011**, *156*, 276-280.

71. Foote, C.S. Definition of Type I and Type II photosensitized oxidation. *Photochem. Photobiol.* **1991,** *54*, 659.

72. Krasnovsky Jr., A.A. Photodynamic action and singlet oxygen, *Biophys. (Mosc.)*, **2004**, *49*, 289–306.

73. Moulder, J.E.; Rockwell, S. Tumor hypoxia: its impact on cancer therapy. *Cancer Metastasis Rev.* **1987**, *5*, 313–341.

74. Pogue, B.W.; Braun, R.D.; Lanzen, J.L.; Erickson, C.; Dewhirst, M.W. Analysis of the heterogeneity of pO_2 dynamics during photodynamic therapy with verteporfin. *Photochem. Photobiol.* **2001**, *74*, 700–706.

75. Vakrat-Haglili, Y.; Weiner, L.; Brumfeld, V.; Brandis, A.; Salomon, Y.; McIlroy, B.; Wilson, B.C.; Pawlak, A.; Rozanowska, M.; Sarna, T.; Scherz, A. The microenvironment effect on the generation of reactive oxygen species by Pd-bacteriopheophorbide. *J. Am. Chem. Soc.* **2005**, *127*, 6487–6497.

76. Singlet oxygen luminescence as an in vivo photodynamic therapy dose metric: validation in normal mouse skin with topical amino-levulinic acid. *British Journal of Cancer*. **2005**, *92(2)*, 298 – 304.

77. Jordan, B.F.; Sonveaux, P. Targeting Tumor Perfusion and Oxygenation to Improve the Outcome of Anticancer Therapy. *Frontiers in Pharmacology Rev.*. **2012**, *3(94)*, 1-15.

78. Jain, R.K. Delivery of molecular and cellular medicine to solid tumors. *Adv. Drug. Deliv. Rev.* **2012,** *64*, 353–365.

79. Khlebtsov, B.; Panfilova, E.; Khanadeev, V.; Bibikova, O.; Terentyuk, G.; Ivanov,A.; Rumyantseva, V.; Shilov, I.; Ryabova, A.; Loshchenov, V.; Khlebtsov, N.G. Nanocomposites Containing Silica-Coated GoldSilver Nanocages and Yb2,4-Dimethoxyhematoporphyrin: Multifunctional

Capability of IR-Luminescence Detection, Photosensitization, and Photothermolysis. *ACS Nano*. **2011**, *5(9)*, 7077-7089.

80. Li, Y.; Zhang, W.; NIu, J.; Chen, Y. Mechanism of Photogenerated Reactive Oxygen Species and Correlation with the Antibacterial Properties of Engineered Metal-Oxide Nanoparticles. *ACS Nano*. **2012**, *6 (6)*, 5164-5173.

6. SUPPORTING INFORMATION

Supporting Information Available: HRTEM particle size distribution of $CuInSe_2$ core QDs and $CuInSe_2$/ZnSe core/shell QDs, HRTEM of $CuInSe_2$/ZnSe core/shell QDs show interphase between $CuInSe_2$ core and ZnSe shell, The Fourier-transform infrared (FT-IR) spectra of $CuInSe_2$/ZnSe core/shell QDs synthesized, PL spectra $CuInSe_2$/ZnSe core/shell quantum dots and photostability exhibited during six months. This material is available free of charge via the Internet at: http://pubs.acs.org.

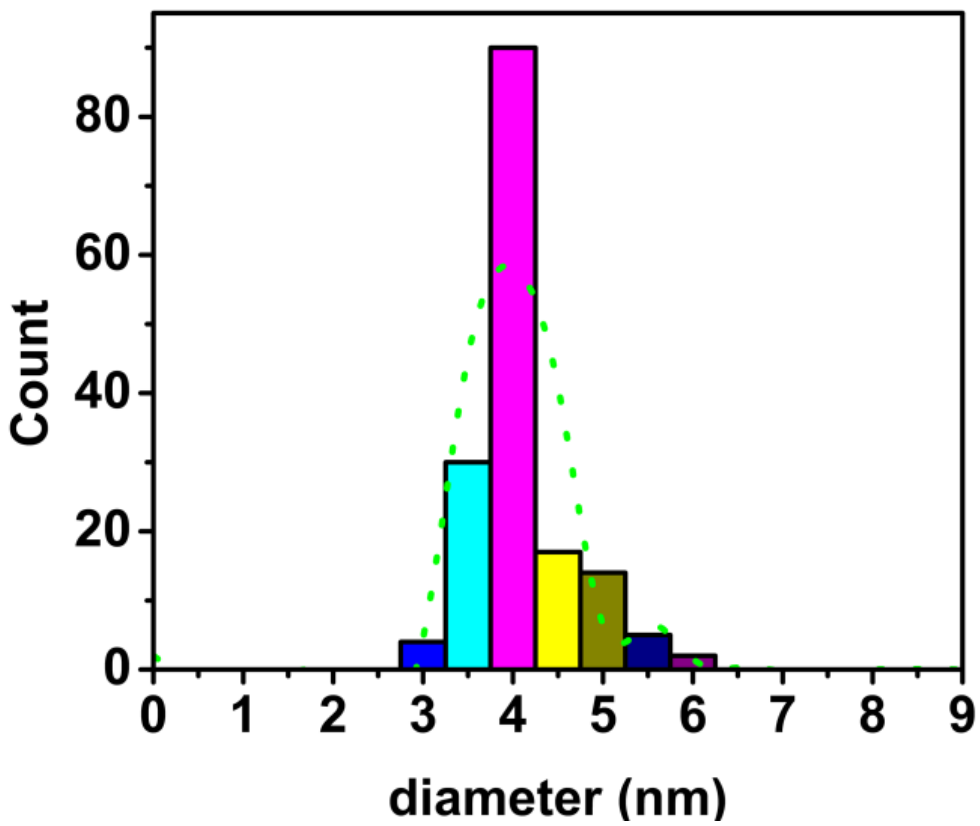

Figure S1. HRTEM particle size distribution of $CuInSe_2$ core QDs: (4±1)nm

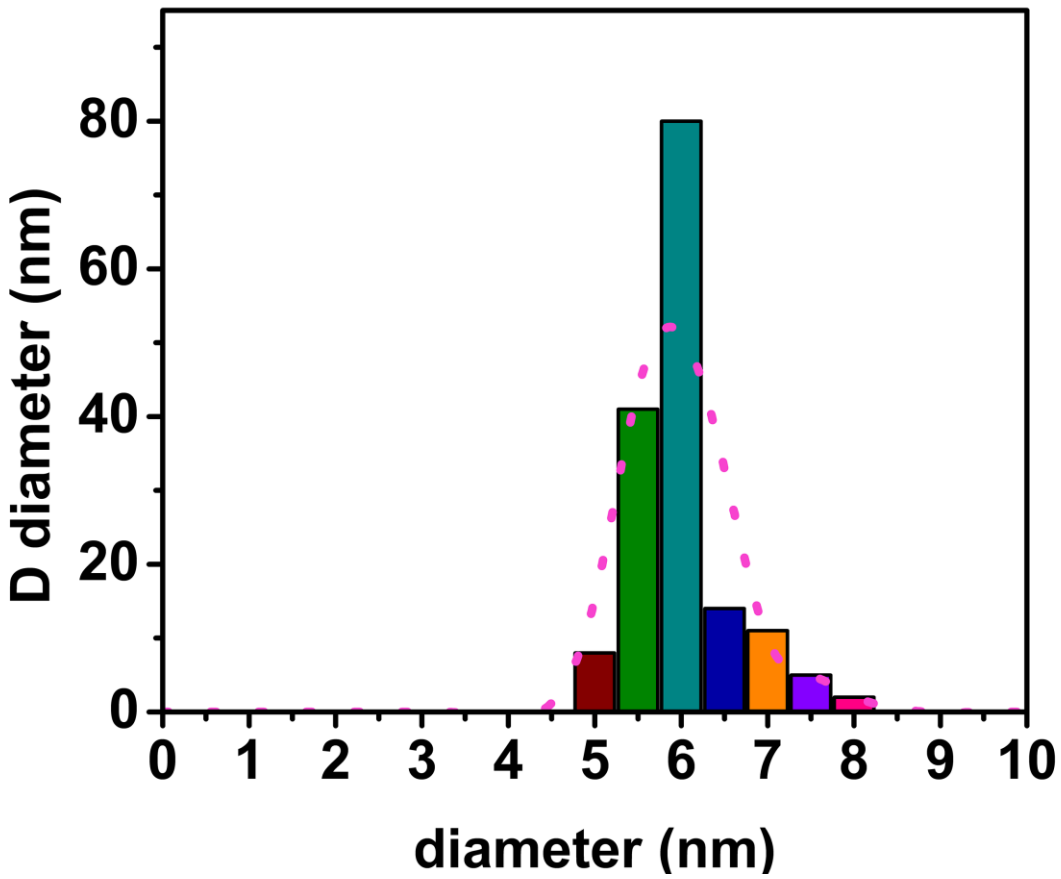

Figure S2. HRTEM particle size distribution of $CuInSe_2$/ZnSe core/shell QDs: (6±1)nm

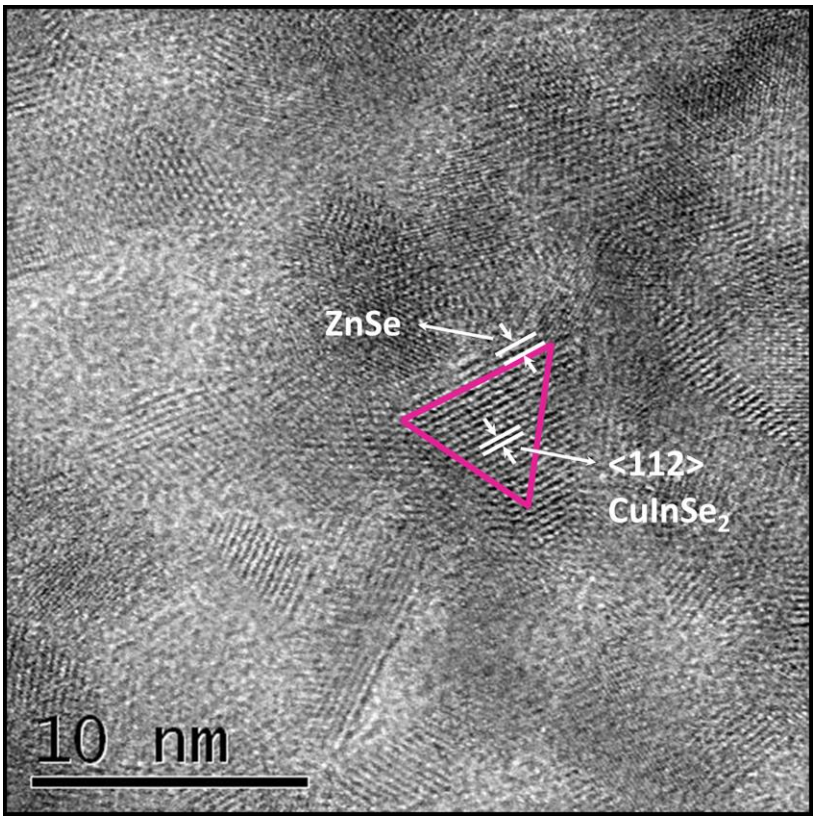

Figure S3.HRTEM of $CuInSe_2$/ZnSe core/shell QDs show interphase between $CuInSe_2$ core and ZnSe shell. The lattice fringes with a distance of 0.334 nm and constant lattice spacing and clear crystal planes evidence the crystal morphology of $CuInSe_2$ core CuInSe2/ZnSe core/shell structures [44-47].

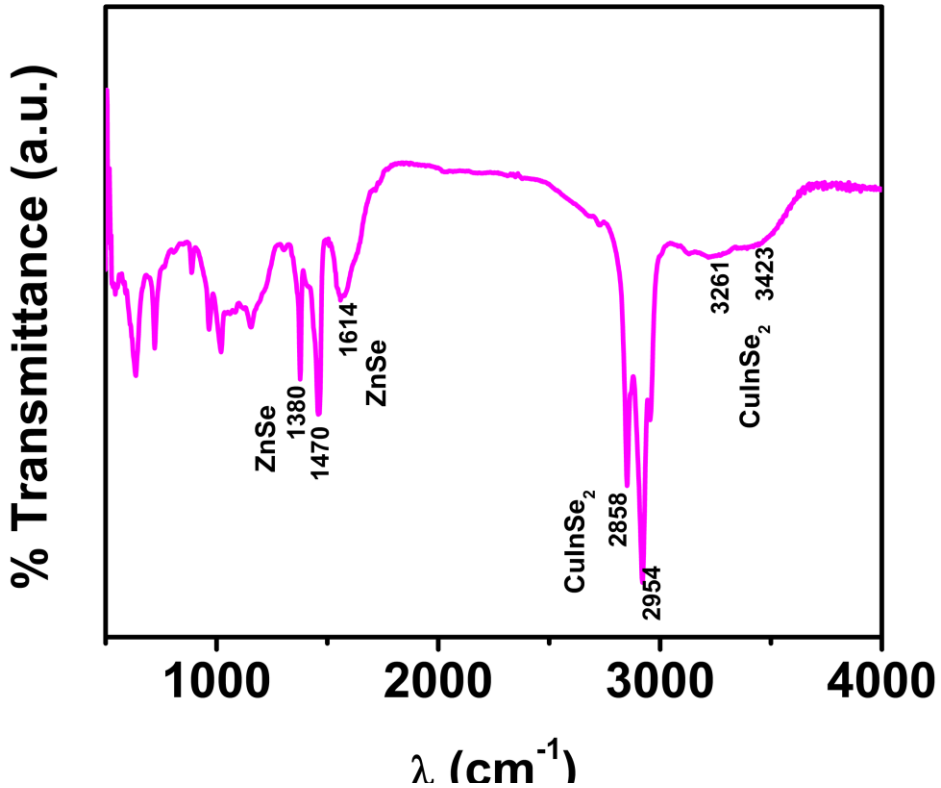

Figure S4. The Fourier-transform infrared (FT-IR) spectra of $CuInSe_2$/ZnSe core/shell QDs synthesized. It is shown that distinct absorption peaks are observed at (2858, 2954,3261, 3423)cm−1, which corresponds to $CuInSe_2$, and (1380, 1614)cm−1). Films of samples were studied in Shimadzu FTIR-8400: Fourier Transform Infrared Spectrophotometer Shimadzu FTIR-8400.

Saikia, K.; Deb, P.; Kalita, E. Sensitive fluorescence response of ZnSe(S) quantum dots: an efficient fluorescence probe. *Phys.Scr.* **2013**, *87*, 065802.

Kashyout, A.E-H.B.; Ahmed, E.-Z.; Meaz, T.; Nabil, M.; Amer, M. (One-step) electrochemical deposition and characterization of $CuInSe_2$ thin films. *Alexandria Eng. J.* **2014**, , http://dx.doi.org/10.1016/j.aej.2014.03.015 (in press).

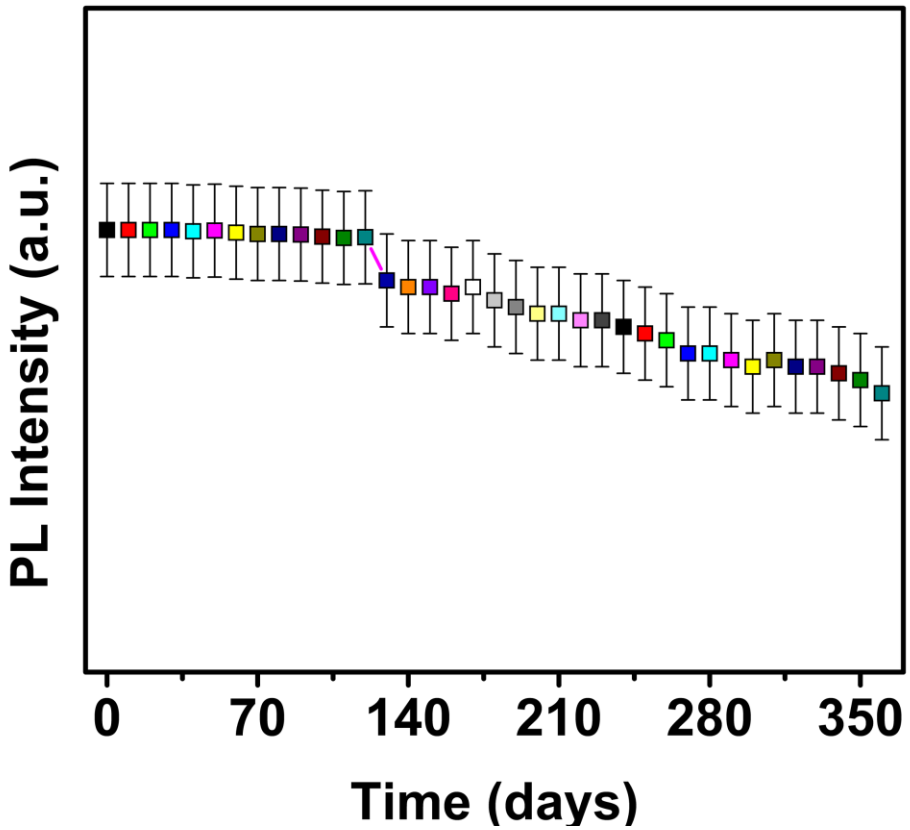

Figure S5A. Photostability exhibited by $CuInSe_2$/ZnSe core/shell QDs during six months. All samples was suspended in hexane and storage in dark conditions to preserve PL properties. The PL experiments were the same to the samples characterization signal in experimental methods section.

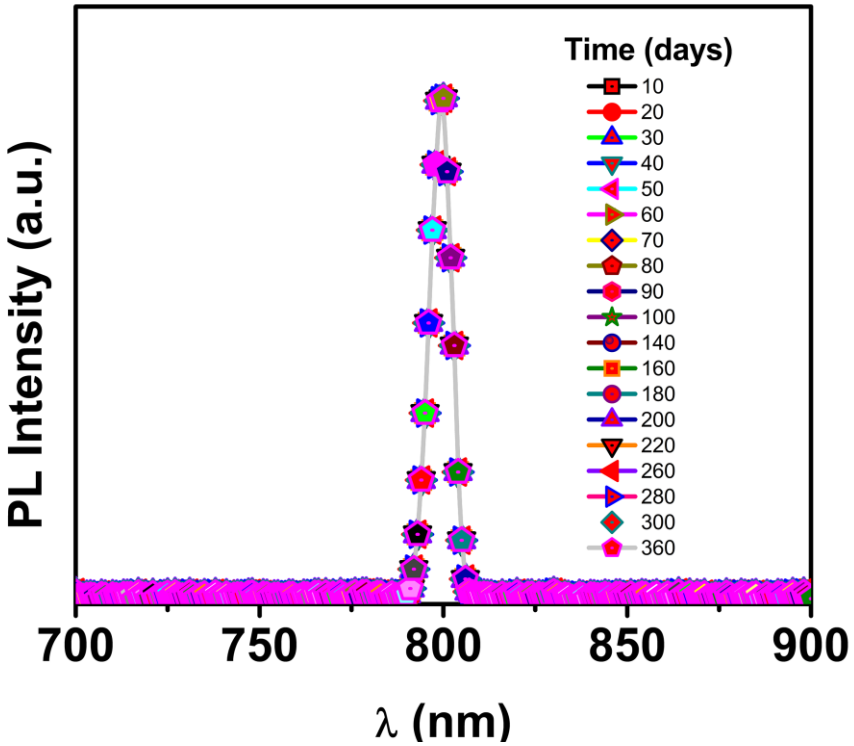

Figure S5B. PL spectra $CuInSe_2$/ZnSe core/shell quantum dots synthesized where exhibited photostability during six months without aggregation.